Author/s:
Hoare, BL;Bruell, S;Sethi, A;Gooley, PR;Lew, MJ;Hossain, MA;Inoue, A;Scott, DJ;Bathgate, RAD

Title:
Multi-Component Mechanism of H2 Relaxin Binding to RXFP1 through NanoBRET Kinetic Analysis

Date:
2019-01-25

Citation:
Hoare, B. L., Bruell, S., Sethi, A., Gooley, P. R., Lew, M. J., Hossain, M. A., Inoue, A., Scott, D. J. & Bathgate, R. A. D. (2019). Multi-Component Mechanism of H2 Relaxin Binding to RXFP1 through NanoBRET Kinetic Analysis. Iscience, 11, pp.93-113. https://doi.org/10.1016/j.isci.2018.12.004.

Persistent Link:
https://hdl.handle.net/11343/253658

iScience

CellPress

Article

Multi-Component Mechanism of H2 Relaxin Binding to RXFP1 through NanoBRET Kinetic Analysis

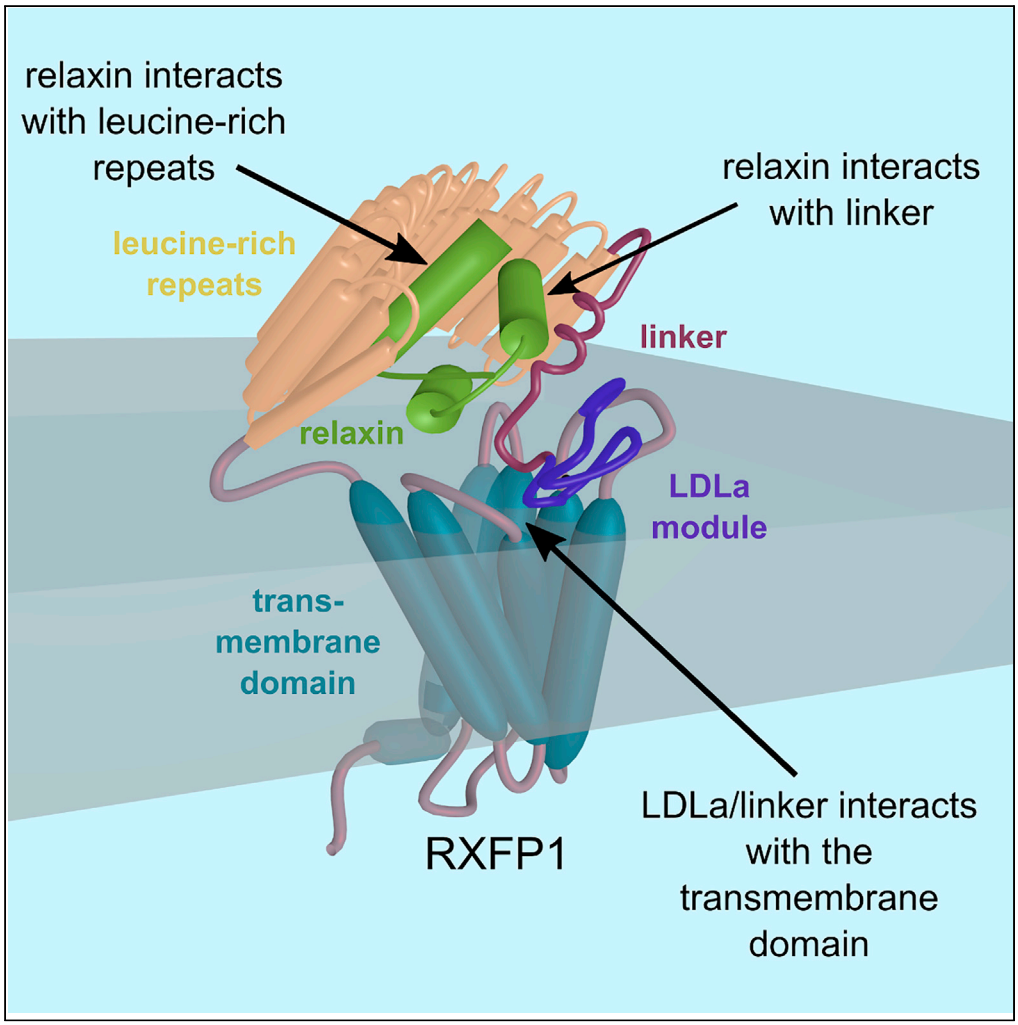

Bradley L. Hoare, Shoni Bruell, Ashish Sethi, ..., Asuka Inoue, Daniel J. Scott, Ross A.D. Bathgate

daniel.scott@florey.edu.au (D.J.S.)
bathgate@florey.edu.au (R.A.D.B.)

HIGHLIGHTS

NanoBRET was used to assess relaxin binding kinetics to its receptor RXFP1

Binding on wild-type and mutant RXFP1 demonstrated a multi-component mechanism

This binding mode was validated using RXFP2/RXFP1 chimeras and protein NMR studies

NanoBRET binding can reveal subtle GPCR binding modes to aid drug development

Hoare et al., iScience *11*, 93–113
January 25, 2019
https://doi.org/10.1016/j.isci.2018.12.004

iScience

CellPress

Article

Multi-Component Mechanism of H2 Relaxin Binding to RXFP1 through NanoBRET Kinetic Analysis

Bradley L. Hoare,[1] Shoni Bruell,[1,2] Ashish Sethi,[2,3] Paul R. Gooley,[2,3] Michael J. Lew,[4] Mohammed A. Hossain,[1,5] Asuka Inoue,[6] Daniel J. Scott,[1,2,*] and Ross A.D. Bathgate[1,2,7,*]

SUMMARY

The peptide hormone H2 relaxin has demonstrated promise as a therapeutic, but mimetic development has been hindered by the poorly understood relaxin receptor RXFP1 activation mechanism. H2 relaxin is hypothesized to bind to two distinct ECD sites, which reorientates the N-terminal LDLa module to activate the transmembrane domain. Here we provide evidence for this model in live cells by measuring bioluminescence resonance energy transfer (BRET) between nanoluciferase-tagged RXFP1 constructs and fluorescently labeled H2 relaxin (NanoBRET). Additionally, we validate these results using the related RXFP2 receptor and chimeras with an inserted RXFP1-binding domain utilizing NanoBRET and nuclear magnetic resonance studies on recombinant proteins. We therefore provide evidence for the multi-component molecular mechanism of H2 relaxin binding to RXFP1 on the full-length receptor in cells. Also, we show the utility of NanoBRET real-time binding kinetics to reveal subtle binding complexities, which may be overlooked in traditional equilibrium binding assays.

INTRODUCTION

Human gene 2 (H2) relaxin (henceforth referred to as "relaxin") is a peptide hormone composed of two peptide chains (A and B chains) linked by two inter-chain and one intra-chain disulphide bond. Initially characterized as a pregnancy hormone with species-dependent roles (Fevold et al., 1930; Bathgate et al., 2006), relaxin has long been of interest as a therapeutic for a number of disease states including cardiovascular (Samuel et al., 2006; Teerlink et al., 2013) and fibrotic disorders (Lekgabe et al., 2005). Around 15 years ago, the receptor mediating the effects of relaxin was identified to be the Class A G protein-coupled receptor (GPCR) originally called LGR7 (Hsu et al., 2002), but now named relaxin family peptide receptor 1 (RXFP1). RXFP1 and the closely related RXFP2, the receptor for insulin-like peptide 3 (INSL3), are large receptors by class A GPCR standards, with an N-terminal extracellular domain (ECD) comprising approximately half of the amino acid sequence. The ECD is made up of at least three protein domains (Figure 1): the LDLa module, linker domain, and leucine-rich repeat (LRR) domain. A thorough understanding of how these domains combine with the transmembrane domain (TMD) to allow relaxin-RXFP1 binding and activation is necessary to rationally design new relaxin-like molecules as therapeutics.

Most Class A GPCR agonists bind directly to the TMD to promote receptor activation and subsequent intracellular signaling events. Conversely, activation of RXFP1 is initiated by relaxin binding to the ECD with coordinated interactions between the LDLa module, linker, and LRR domain driving activation of the TMD. Historically it was believed that the LRR domain is the primary high-affinity relaxin-binding site in the ECD of RXFP1 (Bullesbach and Schwabe, 2005; Scott et al., 2009) with a lower-affinity interaction in the TMD (Halls et al., 2005). However, more recent work has demonstrated that the linker domain has an important role in binding (Sethi et al., 2016). Relaxin can also bind to and activate the related INSL3 receptor, RXFP2, where it binds in a fashion referred to as a hybrid mode, resembling a binding mode somewhere between relaxin-RXFP1 and INSL3-RXFP2 (Bruell et al., 2017). However, RXFP2 lacks the helical stretch of linker thought to bind relaxin and thus has a lower affinity for relaxin. Early work demonstrated that removal of the LDLa module from RXFP1 completely abolished relaxin-mediated signaling but had no effect on relaxin binding affinity (Scott et al., 2006). Site-directed mutagenesis identified key residues within the LDLa, which are proposed to drive receptor activation by forming contacts with the first and second extracellular loops of the TMD (Kong et al., 2013; Diepenhorst et al., 2014). The LDLa module is believed to be a tethered agonist, which interacts with the TMD to promote active receptor-state conformations and

[1]Florey Institute of Neuroscience and Mental Health, The University of Melbourne, Parkville, VIC 3052, Australia

[2]Department of Biochemistry and Molecular Biology, The University of Melbourne, Parkville, VIC, Australia

[3]Bio21 Molecular and Biotechnology Institute, The University of Melbourne, Parkville, VIC, Australia

[4]Department of Pharmacology and Therapeutics, The University of Melbourne, Parkville, VIC 3052, Australia

[5]Department of Chemistry, The University of Melbourne, Parkville, VIC 3052, Australia

[6]Graduate School of Pharmaceutical Sciences, Tohoku University, 6-3, Aoba, Aramaki, Aoba-ku, Sendai, Miyagi 980-8578, Japan

[7]Lead Contact

*Correspondence: daniel.scott@florey.edu.au (D.J.S.), bathgate@florey.edu.au (R.A.D.B.)

https://doi.org/10.1016/j.isci.2018.12.004

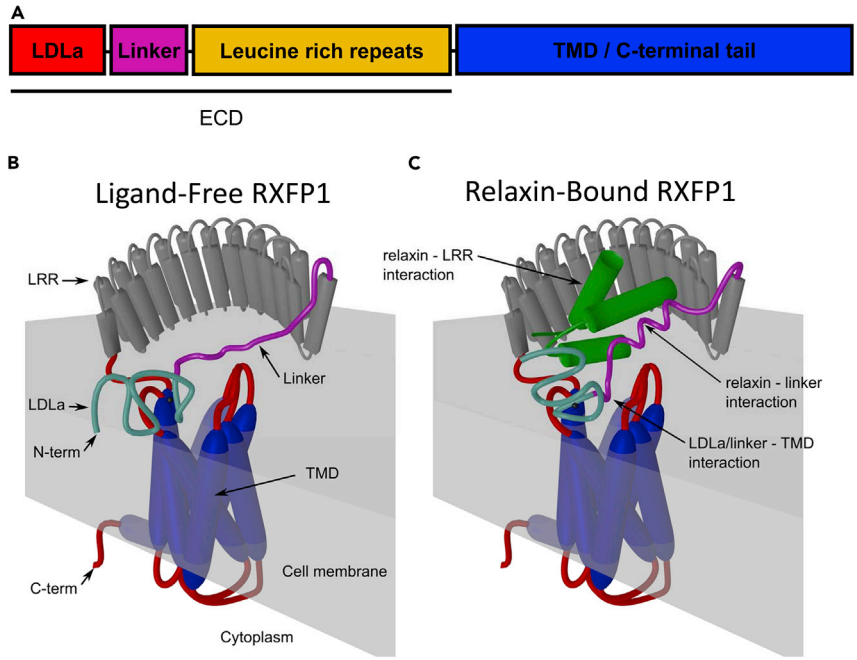

Figure 1. Protein Domains of RXFP1 and RXFP2 and Representative Ligand-free and Ligand-bound RXFP1 Structures

(A) Schematic representation of the protein domains within RXFP1 and RXFP2. (B and C) Cartoon representation of the structure of (B) the ligand-free RXFP1 receptor and (C) the relaxin-bound RXFP1 complex highlighting the coordinated relaxin-leucine-rich repeat (LRR) and relaxin-linker interactions that are necessary to direct LDLa-linker interactions with the transmembrane domain (TMD) that result in receptor activation. Receptor domains and H2 relaxin (green) are labeled and colored; LDLa domain (red), linker domain (magenta), LRR domain (gray), and TMD (blue).

stimulate cell signaling. More recently, it has been demonstrated that the linker domain also plays a key role in activation such that the tethered agonist is now considered to be the combination of LDLa-linker (Sethi et al., 2016; Bruell et al., 2013). Although this indicates some separation between the events of relaxin binding and receptor activation, how these domains combine to form functional RXFP1 proteins has been difficult to study.

This current model of RXFP1 activation is presented in Figure 1 and proposes that relaxin binds the ECD concomitantly over two major sites, with residues in the relaxin B-chain forming contacts with the LRR domain and the A-chain of relaxin potentially interacting with the linker domain. Relaxin binding subsequently promotes the stabilization and extension of an α-helix within the linker domain (Sethi et al., 2016). The resultant structural rearrangement leads to the display of key residues in the LDLa, and potentially the linker domain, to interact with the TMD and agonize the receptor. Recent nuclear magnetic resonance (NMR) studies by our group using purified portions of the LDLa-linker domains gave an estimate of the binding affinity (K_d) of relaxin for the linker domain of about 200 μM (Sethi et al., 2016) and therefore predicted that the binding affinity of relaxin for the LRR domain alone must be around 1 μM to achieve the subnanomolar affinity observed for relaxin binding to the full receptor. It has been challenging to investigate this complex mechanism of relaxin binding across multiple domains in whole cells because of limitations with the traditional ligands used for binding assays, and so the relaxin binding affinity for the LRR domain alone, for example, has not been experimentally determined.

Nanoluciferase (Nanoluc) is a bright luciferase that has gained considerable attention as a useful reporter with a range of research applications (England et al., 2016; Hall et al., 2012). Fusing Nanoluc to the N-termini of GPCRs and measuring bioluminescence resonance energy transfer (BRET) between Nanoluc and a fluorescently labeled ligand (termed NanoBRET; Machleidt et al., 2015) has been proved to be an excellent tool to investigate ligand binding to a variety of GPCRs (Wang et al., 2017; Christiansen et al., 2016; Hansen et al., 2017; Stoddart et al., 2015; Soave et al., 2016) as well as receptor tyrosine kinases (Kilpatrick et al., 2017a, 2017b; Peach et al., 2017). Using NanoBRET for ligand binding has numerous

advantages over traditional ligand-binding assays (Stoddart et al., 2016, 2017)—notably a very low non-specific binding signal, no requirement for removal of unbound fluorescent ligand before measurement, and the potential for easily performing real-time measurements for investigation of binding kinetics.

The investigation of binding kinetics to better understand the mechanism by which a ligand binds its receptor is an area of interest for drug discovery (Tummino and Copeland, 2008; Lu and Tonge, 2010; Swinney et al., 2014). The simplest type of ligand:receptor interaction is the one that occurs via a single reversible step, with the receptor adopting only one bound state (Equation 1).

$$R + L \underset{k_{off}}{\overset{k_{on}}{\rightleftharpoons}} RL \qquad \text{(Equation 1)}$$

Previous reports measuring relaxin association and dissociation rates have assumed a single-step binding mechanism to calculate on- and off-rates (Tan et al., 1999; Kocan et al., 2017) and have only used a single concentration of radioactively labeled relaxin in association experiments, presumably due to the limitations regarding the availability of labeled relaxin and the labor-intensive nature of traditional kinetic ligand-binding assays. Thus real-time measurements of relaxin association to and dissociation from RXFP1 using a technique such as NanoBRET would allow relatively easy kinetic discrimination between a simple one-step binding mechanism and a more complex multi-step binding mechanism, which is currently hypothesized to be occurring.

Here, we describe the development and application of NanoBRET in live HEK293T cells using Nanoluc-tagged RXFP1 and TAMRA-labeled relaxin (TamRLX). Using this technique, we performed NanoBRET saturation binding experiments on several different Nanoluc-RXFP1 constructs in which key receptor domains had been mutated or removed, to dissect the importance of different domains on the overall relaxin binding affinity. A key finding was that, contrary to previously published reports, removal of the N-terminal LDLa domain does perturb relaxin binding to RXFP1. Kinetic experiments revealed complexities that were incompatible with a single-step binding mechanism, and dissociation experiments indicated the existence of at least two relaxin-bound states of RXFP1. To test the hypothesis that the two binding states are associated with the binding sites in the LRR and linker domains, we tested binding to RXFP2, which does not contain the linker-binding site (Bruell et al., 2017), and demonstrated a single-step binding mechanism. In addition, we created chimeric receptors whereby we inserted RXFP1 linker residues into RXFP2 and observed an improvement in both binding and signaling capacity in response to relaxin, as well as a biphasic dissociation profile more similar to that of RXFP1 than of wild-type RXFP2. This finding was supported by data from NMR titrations with relaxin and recombinant LDLa-linker proteins, which highlighted gain of relaxin binding to the linker region in the chimeric RXFP2 protein. Overall, these studies agree with the hypothesized multi-step model of relaxin:RXFP1 binding/activation, highlighting how using the NanoBRET technique that enables kinetic measurements of ligand:receptor binding can reveal subtle, albeit important, effects to aid drug development against this important therapeutic target.

RESULTS

Characterization of TamRLX and Nanoluc-RXFP1

A key aspect of this study was the synthesis of fluorescently labeled relaxin. Labeling relaxin at only one site was important to avoid potentially confounding BRET results. The fluorescent relaxin used here was produced by solid-phase peptide synthesis, with the addition of the orange-red fluorescent dye TAMRA to the N terminus of the A-chain of relaxin via reductive amidation. The ability of TamRLX to activate RXFP1 was tested by using a cyclic AMP (cAMP) reporter gene assay in cells stably expressing RXFP1 (Figure 2A). TamRLX activated RXFP1 with full efficacy compared with relaxin; however, there was a slight decrease in the potency of TamRLX at RXFP1 compared with relaxin (pEC_{50} = 10.06 $\pm$ 0.04 for TamRLX compared with 10.57 $\pm$ 0.03 for relaxin; Table 1).

Nanoluc was tagged to the N-terminus of RXFP1 between a FLAG epitope tag and the LDLa module, and the ability of Nanoluc-RXFP1 to signal when stimulated with relaxin was investigated using the cAMP reporter gene assay. Given the positioning of Nanoluc in the construct and the importance of the LDLa module in receptor activation, this addition was well tolerated, showing only a small, albeit significant, rightward shift of the concentration-response curve compared with RXFP1 (Figure 1C, Table 1; pEC_{50} of 10.71 $\pm$ 0.02 for RXFP1 compared with 10.46 $\pm$ 0.06 for Nanoluc-RXFP1; $p < 0.01$). ML290 is an allosteric agonist of RXFP1 that binds the TMD directly to activate RXFP1 (Kocan et al., 2017; Chen et al., 2013; Xiao et al.,

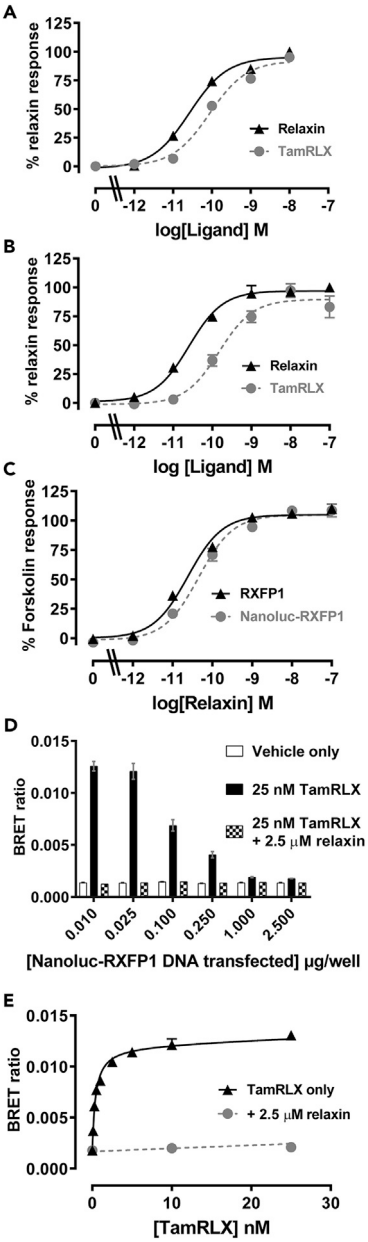

Figure 2. Characterization of TamRLX and Nanoluc-RXFP1 Functional Activity and Use in BRET Experiments

(A and B) Dose-response curves of cAMP activity in HEK293T cells expressing RXFP1 (A) or Nanoluc-RXFP1 (B) when stimulated with relaxin or TamRLX using a cAMP reporter gene system. Pooled data from three to seven independent experiments performed in triplicate.

(C and D) (C) Dose-response curves of cAMP activity in HEK293T cells transiently expressing either RXFP1 or Nanoluc-RXFP1 and stimulated with relaxin, using cAMP reporter gene system. Pooled data from seven to nine independent experiments performed in triplicate. (D) BRET ratio of HEK293T cells transfected with varying amounts of Nanoluc-RXFP1 DNA and incubated with either vehicle or 25 nM TamRLX (±2.5 μM relaxin). Pooled data from four independent experiments performed in duplicate.

(E) NanoBRET saturation binding in HEK293T cells transiently expressing Nanoluc-RXFP1 and incubated with varying concentrations of TamRLX with non-specific signal determined by co-incubation with 2.5 μM relaxin. Determination of K_d is provided in Table 2. Pooled data from four independent experiments performed in duplicate. All error bars (where visible) represent SEM.

Receptor	Relaxin			ML290			INSL3		
	pEC_{50}	E_{max}	n	pEC_{50}	E_{max}	n	pEC_{50}	E_{max}	n
RXFP1	10.71 ± 0.02	109 ± 2.9	9	5.84 ± 0.10	85.6 ± 8.1	3	ND		
NL-RXFP1	10.46 ± 0.06[a]	107 ± 2.1	7	5.90 ± 0.04	99.2 ± 5.9	7	ND		
NL-RXFP1 (ΔLDLa)	No activity		4	5.89 ± 0.03	99.8 ± 2.5	4	ND		
NL-RXFP1 (ΔLDLa/ΔLinker)	No activity		3	5.58 ± 0.02	78.6 ± 4.4	3	ND		
NL-RXFP1-F54A/Y58A	9.57 ± 0.10[b]	104 ± 8.4	3	5.75 ± 0.40	99.0 ± 7.4	3	ND		
NL-RXFP1-E277Q/D279N	No activity		3	5.49 ± 0.09	90.3 ± 15	3	ND		
RXFP2	8.57 ± 0.26[b]	90.1 ± 5.4	3	ND			10.78 ± 0.12	100	3
Nanoluc-RXFP2	8.36 ± 0.12[b]	99.8 ± 9.5	3	ND			ND	ND	
ExLink1	9.48 ± 0.36[a,c]	97.2 ± 37.8	4	ND			10.15 ± 0.15	114.7 ± 7.47	3
ExLink2	9.74 ± 0.24[a,d]	115 ± 27.3	6	ND			10.94 ± 0.16	115 ± 5.45	3

Table 1. Summary of Ligand-Induced cAMP Responses of RXFP1 and RXFP2 Receptors Expressed in HEK293T Cells Utilized in These Studies

NL, Nanoluc; ND, not determined.

[a]$p < 0.01$.

[b]$p < 0.001$ versus RXFP1.

[c]$p < 0.05$.

[d]$p < 0.01$ versus RXFP2.

2013; Huang et al., 2015). Critically, ML290 was able to activate RXFP1 and Nanoluc-RXFP1 with the same potency and efficacy (Table 1). Finally, the combination of TamRLX and Nanoluc-RXFP1 was tested (Figure 2B), showing that TamRLX activates the Nluc-RXFP1 with full efficacy compared with relaxin; however, there was again a small decrease in the potency of TamRLX at Nluc-RXFP1 (pEC_{50} = 9.77 ± 0.07), similar to that seen for TamRLX activation of RXFP1. Nonetheless, the sub-nanomolar potency of TamRLX validated the peptide as a suitable fluorescent ligand for RXFP1 binding studies.

The expression of Nanoluc-RXFP1 was varied by titrating HEK293T cells with varying amounts of Nanoluc-RXFP1-encoding plasmid in transient transfections. Transfected cells were then incubated at room temperature for 90 min with either vehicle or 25 nM TamRLX (with or without 2.5 μM unlabeled relaxin) before adding Nano-Glo (Nanoluc luciferase substrate) to determine if a BRET signal could be detected between Nanoluc and TAMRA. Binding of TamRLX to Nanoluc-RXFP1 produced a strong BRET signal with negligible non-specific binding signal, and we found that the highest NanoBRET binding signal was produced with the lowest expression levels (Figure 2D), and thus used lower transfection levels (10–30 ng/well) for all subsequent NanoBRET experiments.

We then performed a saturation binding experiment by incubating varying concentrations of TamRLX (0–25 nM) with Nanoluc-RXFP1-expressing HEK293T cells and determined non-specific signal by co-incubation with an excess of unlabelled relaxin. This yielded an excellent quality of fit to a one-site binding isotherm (Figure 2E; K_d = 0.42 ± 0.03 nM), in line with that previously reported in the literature (Halls et al., 2005; Shabanpoor et al., 2012; Sethi et al., 2016).

NanoBRET Saturation Binding Assays to Investigate the Multiple Binding Domains of RXFP1

Relaxin is believed to bind to the ECD of RXFP1 simultaneously across two distinct domains: the LRR and linker domains. We therefore cloned several different mutant and chimeric Nanoluc-RXFP1 constructs, which were rationally chosen to dissect the importance of these key domains for overall relaxin binding affinity. Importantly, all the RXFP1 mutant receptors demonstrated no changes in ligand potency or efficacy of the small molecule allosteric agonist ML290, highlighting that the receptors were able to couple to G protein and were expressed at the cell surface normally (Table 1).

The primary high-affinity binding interaction between relaxin and RXFP1 is believed to be between arginine residues B13 and B17 in the relaxin B-chain, which form ionic interactions with acidic residues E277/D279

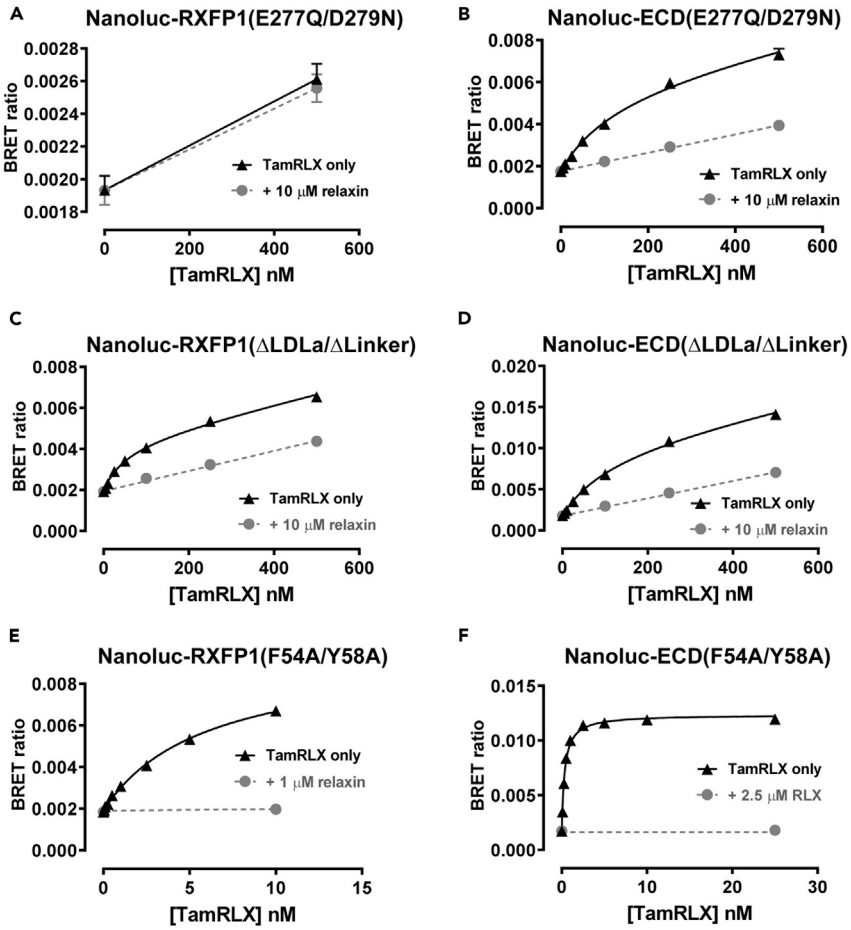

Figure 3. NanoBRET Saturation Binding on RXFP1 and ECD-Only Constructs

Hek293T cells transiently expressing Nanoluc-tagged constructs (A) Nanoluc-RXFP1(E277Q/D279N), (B) Nanoluc-ECD(E277Q/D279N), (C) Nanoluc-RXFP1(ΔLDLa/ΔLinker), (D) Nanoluc-ECD(ΔLDLa/ΔLinker), (E) Nanoluc-RXFP1(F54A/Y58A), (F) Nanoluc-ECD(F54A/Y58A) incubated with varying concentrations of TamRLX with non-specific signal determined by co-incubation an excess of unlabelled relaxin.

and D231/E233 in the LRR domain of RXFP1, respectively (Bullesbach and Schwabe, 2005). We found that mutating just one of these pairs of acidic residues (Nanoluc-RXFP1-E277Q/D279N) was enough to abolish any detectable TamRLX binding up to a concentration of 500 nM (Figure 3A). This lack of binding was associated with no cAMP activity in response to relaxin (Table 1). Interestingly, when we applied this mutation to a construct encoding only the ECD of RXFP1 attached to a membrane anchor (previously termed 7BP; Hsu et al., 2002), TamRLX was able to bind with reasonable affinity (Figure 3B; K_d = 136 ± 10 nM).

Using the ECD-only construct and removing the LDLa/linker domains (Nanoluc-ECD [ΔLDLa/ΔLinker]), we were able to estimate the binding affinity of TamRLX for the LRR domain alone to be 121 ± 5.9 nM (Figure 3D). When the TMD was reintroduced (Nanoluc-RXFP1(ΔLDLa/ΔLinker)) the affinity for TamRLX was improved (Figure 3C; K_d = 58 ± 13 nM).

We also applied a previously characterized linker domain mutation, F54A/Y58A, which results in a 10-fold decrease in both relaxin binding and activation (Sethi et al., 2016). In our NanoBRET saturation binding studies, TamRLX also exhibited a 10-fold reduction in binding to Nanoluc-RXFP1-F54A/Y58A (Figure 3E; K_d = 5.8 ± 0.28 nM) compared with Nanoluc-RXFP1. Conversely, the affinity of TamRLX for the ECD-only construct with this mutation (Figure 3F; K_d = 0.34 ± 0.01 nM) was not different from its affinity for Nanoluc-ECD (Figure 4B; K_d = 0.28 ± 0.01 nM).

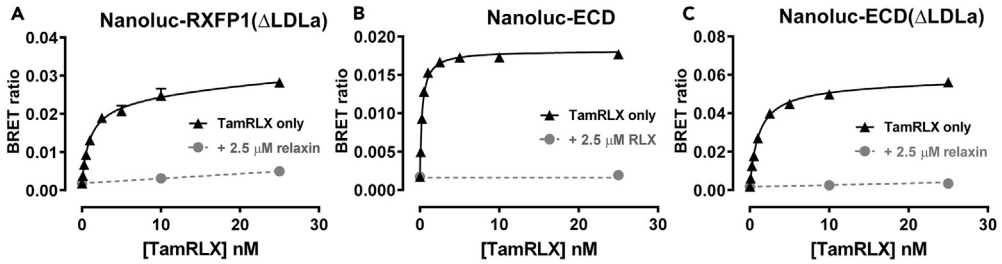

Figure 4. NanoBRET Saturation Binding on RXFP1 and ECD-Only Constructs Lacking the LDLa Domain

Hek293T cells transiently expressing Nanoluc-tagged constructs (A) Nanoluc-RXFP1(ΔLDLa), (B) Nanoluc-ECD, (C) Nanoluc-ECD(ΔLDLa/ΔLinker) incubated with varying concentrations of TamRLX with non-specific signal determined by co-incubation 2.5 μM relaxin.

NanoBRET Saturation Binding Assays to Probe the Role of the LDLa on Relaxin Binding

Studies have clearly shown that relaxin does not have direct binding interactions with the LDLa (Hopkins et al., 2007; Sethi et al., 2016), and removing or altering the LDLa module from RXFP1 does not appear to affect the relaxin binding affinity (Scott et al., 2006; Hopkins et al., 2007; Kong et al., 2013). We were therefore surprised to observe a statistically significant reduction in the affinity of TamRLX for RXFP1 with the LDLa module deleted (Figure 4; Table 2; K_d = 0.42 ± 0.03 nM for Nanoluc-RXFP1 versus K_d = 1.10 ± 0.09 nM for Nanoluc-RXFP1(ΔLDLa); $p < 0.001$).

TamRLX binding affinity for the ECD-only version of these constructs were similarly decreased (Figures 4B and 4C; K_d = 0.28 ± 0.013 nM for Nanoluc-ECD versus K_d = 1.1 ± 0.13 nM for Nanoluc-ECD(ΔLDLa); $p < 0.001$). This suggests that the LDLa plays a subtle role in modulating how relaxin binds to the LRRs and linker domain, which is independent of potential interactions with the TMD.

The results on RXFP1-ECD constructs suggest that the lack of TMD, and therefore lack of G protein coupling, has no influence on the relaxin binding affinity. However, there are some distinct differences in the binding of relaxin to the ECD constructs, hence we wanted to clearly demonstrate that G protein coupling has no influence on the relaxin binding affinity. We therefore performed the same saturation binding assays in both HEK293T cells and a HEK293 cell line in which the $G_{\alpha s}$ subunit had been knocked out (HEK293A $\Delta G_{\alpha s}$; Stallaert et al., 2017) at a physiological temperature (37°C). At this temperature, we found that the relaxin binding affinity for Nanoluc-RXFP1 decreased compared with that at room temperature, but that LDLa removal also resulted in similarly small decreases in TamRLX binding affinity (Figures 5A and 5B; K_d = 3.20 ± 0.02 nM for Nanoluc-RXFP1 versus K_d = 5.8 ± 1.2 nM for Nanoluc-RXFP1(ΔLDLa)). This was also true in the HEK293A $\Delta G_{\alpha s}$ knockout cells (Figures 5C and 5D), and there were no significant differences in TamRLX binding affinity between cell types. This further supported the notion that the subtle decrease in relaxin binding affinity when the LDLa was removed was due to interactions at the level of the ECD rather than related to LDLa interactions activating the TMD.

NanoBRET Association Assays to Investigate the Influence of the LDLa Module on the Kinetics of Relaxin Binding to RXFP1

An advantage of NanoBRET compared with traditional ligand binding assays is the possibility to perform real-time measurements of ligand binding kinetics. Measuring the rates of ligand association and dissociation directly can provide valuable insight into binding mechanisms, which may be obscured when relying on binding measurements obtained at equilibrium. Identification of subtle differences in TamRLX binding may provide insight into the hypothesized mechanism of RXFP1 binding, so we looked more closely at the TamRLX binding kinetics at Nanoluc-RXFP1 and Nanoluc-RXFP1(ΔLDLa).

Association assays were performed using TamRLX concentrations ranging between 0.25 and 5 nM (Figure 6A). The association profiles fit well to one-phase exponential functions, which gave pseudo-first-order association rates (k_{obs}). Based on the assumption that this binding occurs via a single-step mechanism, k_{obs} is related to the concentration of TamRLX ([TamRLX]) by Equation 2.

$$k_{obs} = k_{on}[\text{TamRLX}] + k_{off} \qquad \text{(Equation 2)}$$

NL-Tagged Receptors	K_d (nM) Room Temperature HEK293T	K_d (nM) 37°C HEK293T	K_d (nM) 37°C HEK293A ΔGαs
RXFP1	0.42 ± 0.03 (4)	3.2 ± 0.3 (3)	2.3 ± 0.1 (3)
RXFP1 (ΔLDLa)	1.1 ± 0.09 (3)[a]	5.0 ± 0.2 (3)[b]	5.8 ± 0.5 (3)[c]
RXFP1 (ΔLDLa/ΔLinker)	58 ± 13 (3)[a]	–	–
RXFP1-E277Q/D279N	No binding	–	–
RXFP1-F54A/Y58A	5.4 ± 0.3 (3)[a]	–	–
ECD	0.28 ± 0.01 (3)	–	–
ECD (ΔLDLa)	1.1 ± 0.13 (3)[d]	–	–
ECD (ΔLDLa/ΔLinker)	121 ± 5.9 (3)[d]	–	–
ECD-E277Q/D279N	136 ± 10 (3)[d]	–	–
ECD-F54A/Y58A	0.34 ± 0.01 (3)	–	–
RXFP2	10.74 ± 1.64 (4)	–	–
ExLink1	2.74 ± 0.52 (4) [e]	–	–
ExLink2	1.17 ± 0.2 (4) [e]	–	–

Table 2. Summary of NanoBRET Saturation Binding K_d Determinations for the Nanoluc-Tagged Receptors Used in This Study

The number of experimental replicates for each individual construct are shown in parentheses.

[a]p< 0.001 versus Nanoluc-RXFP1.

[b]p< 0.01 versus Nanoluc-RXFP1 in HEK293T cells at 37°C.

[c]p< 0.001 versus Nanoluc-RXFP1 in HEK293A $\Delta G_{\alpha s}$ cells at 37°C.

[d]p< 0.001 versus Nanoluc-ECD.

[e]p< 0.0001 compared with Nanoluc-RXFP2.

Compatible with this assumption, the k_{obs} versus TamRLX concentration plot showed a linear relationship (Figure 6B), allowing determination of k_{on} and k_{off} by linear regression (Table 3). The calculated k_{off} and k_{on} for TamRLX at Nanoluc-RXFP1 was 0.054 ± 0.009 min^{-1} and 0.046 ± 0.004 $nM^{-1}.min^{-1}$, respectively. Comparatively, the binding of TamRLX to Nanoluc-RXFP1(ΔLDLa) showed differences in both on- and off-rates (k_{on}= 0.026 ± 0.005 $nM^{-1}.min^{-1}$; k_{off} = 0.249 ± 0.012 min^{-1}), which is consistent with the lower binding affinity seen in saturation binding experiments.

The calculated K_d (= k_{off}/k_{on}) from these association experiments were 1.2 ± 0.23 nM for TamRLX at Nanoluc-RXFP1 and 9.6 ± 1.8 nM at Nanoluc-RXFP1(ΔLDLa). If the assumption of a one-step binding mechanism is valid, these results should closely match those observed in equilibrium saturation binding assays; however, the calculated K_d for TamRLX at Nanoluc-RXFP1(ΔLDLa) was almost 10-fold different from that obtained in saturation binding. Additionally, the finding that TamRLX has a lower k_{on} at Nanoluc-RXFP1(ΔLDLa) was unexpected because on-rates are usually linked to the diffusional characteristics of the ligand, which remained constant. These inconsistencies suggest that the assumption of a one-step binding mechanism is invalid, providing support for a more complex binding mode.

NanoBRET Dissociation Assays to Investigate the Influence of the LDLa Module on the Kinetics of Relaxin Binding to RXFP1

Owing to the presence of two binding sites, we hypothesized that relaxin binding and activation of RXFP1 involves at least two steps. Thus it is reasonable to suggest that the dissociation profile of relaxin from RXFP1 may show at least two distinct phases, indicative of at least two relaxin-bound states at the receptor. Previous studies that have measured relaxin dissociation from RXFP1 have generally fit dissociation curves to one-phase decay functions; however, we speculated that the sensitivity and superior temporal resolution afforded by the NanoBRET system might allow reliable detection and quantitation of multiple off-rates.

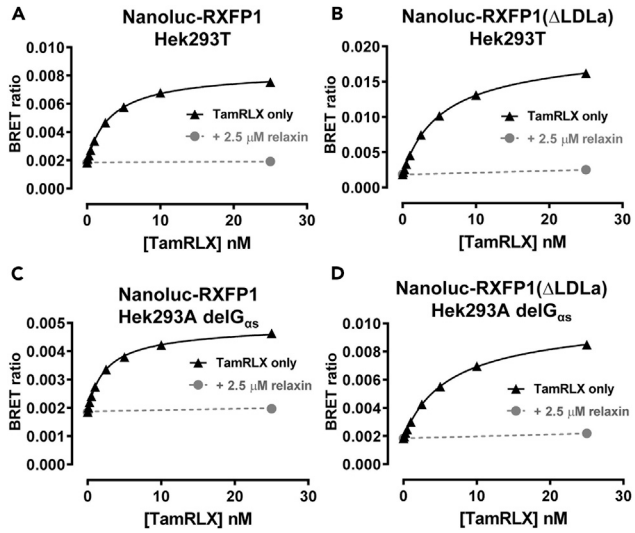

Figure 5. NanoBRET Saturation Binding at 37°C in Hek293T and Hek293AdelG$_{\alpha s}$

Cells transiently expressing Nanoluc-RXFP1 (A and C) or Nanoluc-RXFP1(ΔLDLa) (B and D) were incubated at 37°C with varying concentrations of TamRLX with non-specific signal determined by co-incubation 2.5 μM relaxin. A comparison was made between receptor expression in Hek293T (A and B) and Hek293AdelG$_{\alpha s}$ (C and D). Pooled data from three independent experiments performed in duplicate. All error bars (where visible) represent SEM. All K_d determinations are provided in Table 2.

Dissociation experiments were performed at room temperature in HEK293T cells expressing Nanoluc-tagged receptors and involved binding 1 nM TamRLX to equilibrium for 1 hr, followed by removal of unbound TamRLX from the well and addition of 10 μM unlabeled relaxin. The BRET ratios were normalized to wells containing vehicle only (0%) and wells in which 1 nM TamRLX remained (100%). This was done to remove the potentially confounding effect of BRET signal decay, which was evident over long time periods (Figure S1).

TamRLX dissociated from Nanoluc-RXFP1 more slowly than from Nanoluc-RXFP1(ΔLDLa) (Figure 7A). Both dissociation profiles were found to fit best to a two-phase exponential decay function, as can be seen in the time-invariant distribution of residuals for the two-phase models (Figures 7B–7E). The fast and slow off-rate estimates were the same for both constructs (Table 3; $k_{offFAST}$ = 0.15 ± 0.05 min^{-1}, $k_{offSLOW}$ = 0.021 ± 0.003 min^{-1} for Nanoluc-RXFP1; $k_{offFAST}$ = 0.16 ± 0.02 min^{-1}, $k_{offSLOW}$ = 0.026 ± 0.009 min^{-1} for Nanoluc-RXFP1(ΔLDLa)). The overall slower dissociation from Nanoluc-RXFP1 can be explained by it having a lower proportion of the fast dissociation component (around 19% for Nanoluc-RXFP1 compared with 61% for Nanoluc-RXFP1(ΔLDLa)). This suggested that the same two relaxin-bound states can exist when the LDLa domain is removed and that the LDLa may help to stabilize the higher affinity-bound state.

NanoBRET Dissociation Assays at 37°C to Further Validate the Role of the LDLa in Relaxin Binding Interactions with the ECD

The physiological relevance of two relaxin-bound states was further investigated by obtaining TamRLX dissociation profiles at 37°C (Figure 8). Dissociation was initiated by automated injection of a 1,000-fold excess of unlabeled relaxin to accurately capture the expected faster dissociation at a higher temperature rather than by manual handling of the plate to remove unbound TamRLX. This was deemed suitable as there was no difference in TamRLX off-rates at room temperature when 10 μM unlabeled competitor relaxin was added, regardless of whether unbound TamRLX was removed or not (Figure S2). Here, the TamRLX dissociation from Nanoluc-RXFP1 again fit best to a two-phase exponential decay (Table 3; $k_{off\ FAST}$ = 0.19 ± 0.01 min^{-1}; $k_{off\ SLOW}$ = 0.044 ± 0.008 min^{-1}); however, the faster off-rate accounted for a larger percentage of the overall dissociation profile (around 67% at 37°C compared with 20% at room temperature). The dissociation of TamRLX from Nanoluc-RXFP1(ΔLDLa) was clearly faster compared with that from Nanoluc-RXFP1 (Figure 8A); however, we fit the data to a one-phase exponential as a two-phase exponential did not improve the quality of the fit. Interestingly, this monophasic off-rate for Nanoluc-RXFP1(ΔLDLa)

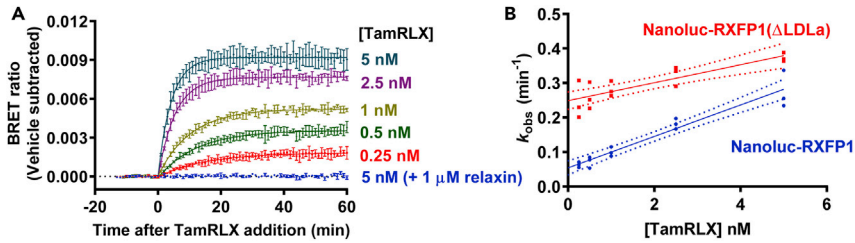

Figure 6. NanoBRET Association Experiments in Nanoluc-Receptor-Expressing HEK293T Cells

(A) Representative figure of a single experiment with HEK293T cells transiently expressing Nanoluc-RXFP1 and treated with varying concentrations of TamRLX. Curves fit to a one-phase association equation in GraphPad Prism to obtain k_{obs} values. Experiments performed in triplicate, and error bars represent SEM.

(B) Pooled k_{obs} from three independent association experiments for Nanoluc-RXFP1 and Nanoluc-RXFP1(ΔLDLa), plotted as a function of TamRLX concentration and fit to a linear regression in GraphPad Prism. Dotted line indicates 95% confidence interval of the linear regression, and each point represents a single k_{obs} determination from one experiment. On- and off-rate determinations from linear fit are provided in Table 3, based on the relationship $k_{obs} = k_{on}.[TamRLX] + k_{off}$.

was 0.20 ± 0.004 min^{-1}, corresponding to the fast off-rate for TamRLX dissociation from Nanoluc-RXFP1. Additionally, the residuals plots for both fits used (two phase for RXFP1, Figure 8D; one phase for RXFP1(ΔLDLa), Figure 8C) show movement above and below the line in the first 10 min of dissociation, which may indicate additional complexity that was not fit by these models.

NanoBRET Saturation Binding Assays to Investigate the Binding of Relaxin to RXFP2 and Chimeric Linker Insertion Mutants

To test the hypothesis that the two binding states of RXFP1 are associated with the binding sites in the LRRs and the linker domain, we conducted binding studies on RXFP2, which does not contain the linker-binding site (Bruell et al., 2017). We therefore first cloned a Nanoluc tag at an equivalent position of FLAG-tagged RXFP2 to Nanoluc-RXFP1, and the resulting Nanoluc-RXFP2 construct was tested for cAMP activity in response to relaxin in the same way (Figure 9A). Relaxin potency at Nanoluc-RXFP2 was not significantly different from RXFP2 (Table 1), and similarly, the potency of TamRLX was not significantly different from relaxin at RXFP2 (Figure 9B; EC_{50} = 8.46 ± 0.25 versus 8.57 ± 0.26). We previously reported the affinity of relaxin for RXFP2 as being around 10 nM using a saturation binding assay with europium-labeled H2 relaxin (Bruell et al., 2017). Similarly, here using the NanoBRET system with Nanoluc-RXFP2 titrated with TamRLX, we demonstrated that the K_d was 10.74 ± 1.64 nM (Figure 9C).

To further highlight the role of the linker-binding site, we created chimeric receptors whereby we inserted four or seven residues from the proposed RXFP1-relaxin-binding site (Sethi et al., 2016) into the RXFP2 linker to produce the chimeras named Nanoluc-ExLink1 (four-residue insertion) and Nanoluc-ExLink2 (seven-residue insertion; Figure 10A). Both Nanoluc tagged and non-tagged versions of the constructs were cloned for testing of TamRLX saturation binding and relaxin cAMP potency, respectively. Both chimeric constructs showed a significantly increased affinity for TamRLX in NanoBRET saturation binding assays (Figures 10C and 10D; Table 2; $p<0.0001$ compared with RXFP2 for both). This improved affinity was matched with significantly increased potency of relaxin at both receptors compared with RXFP2 (Figure 10B; Table 1; $p < 0.05$ and $p < 0.01$ versus RXFP2, respectively). Importantly, both chimeric constructs responded normally to the RXFP2 cognate ligand INSL3, which is known to not bind to the linker site (Bruell et al., 2017) (Figure 10C; Table 1). The results support the notion of an additional relaxin-binding site being present in the RXFP1, but not in the RXFP2 linker.

NanoBRET Dissociation Assays to Compare the Kinetics of Relaxin Binding to RXFP2 with RXFP1

Given that the linker residues joining the LDLa module to the LRRs are a major point of difference between the highly similar RXFP1 and RXFP2 receptors, we compared the TamRLX dissociation profile of the RXFP2 and the ExLink chimeric receptors (Figure 11). TamRLX dissociation from Nluc-RXFP2 was best fit to a one-phase exponential (k_{off} = 0.43 ± 0.05 min^{-1}; Figures 11A, 11C, and 11F), indicative of a single binding site for relaxin in the RXFP2 LRRs. Introduction of the RXFP1-linker-binding site in the ExLink1 and ExLink2

NL-Tagged Receptor	Association Experiments			Dissociation Experiments			Dissociation Experiments (37°C)		
	k_{on} ($nM.min^{-1}$)	k_{off} (min^{-1})	K_d (k_{off}/k_{on}) (nM)	$k_{off\ FAST}$ (min^{-1})	$k_{off\ SLOW}$ (min^{-1})	Fast Component (%)	$k_{off\ FAST}$ (min^{-1})	$k_{off\ SLOW}$ (min^{-1})	Fast Component (%)
RXFP1	0.046 ± 0.004	0.054 ± 0.009	1.2 ± 0.23	0.15 ± 0.05	0.021 ± 0.003	19 ± 4	0.19 ± 0.01	0.044 ± 0.008	67 ± 5
RXFP1 (ΔLDLa)	0.026 ±0.005	0.25 ±0.01	9.6 ±1.8	0.16 ±0.02	0.026 ±0.009	61 ± 6	[a]0.20 ±0.004	–	–
RXFP2	–	–	–	[a]0.43 ± 0.05	–	–	–	–	–
ExLink1	–	–	–	0.46 ± 0.05	0.04 ± 0.01	79 ± 1	–	–	–
ExLink2	–	–	–	0.47 ± 0.09	0.085 ± 0.03	49 ± 12	–	–	–

Table 3. Pooled Kinetic Parameters from NanoBRET Kinetic Experiments in HEK293T Cells

Rate constant determinations from RXFP1 association experiments (Figure 5), RXFP1 dissociation experiments (Figure 6), RXFP1 dissociation experiments at 37°C (Figure 7), and RXFP2 dissociation experiments (Figure 11).

NL, Nanoluc.

[a]k_{off} from a one-phase decay fit.

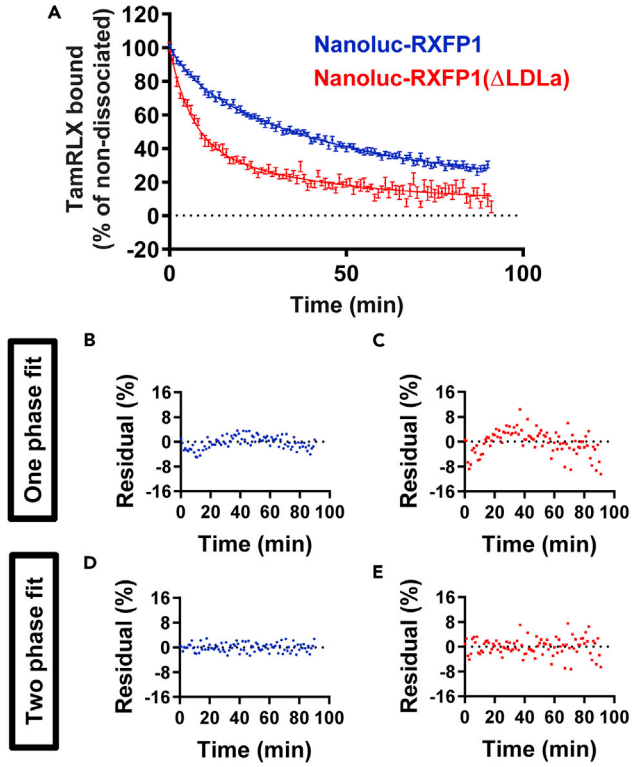

Figure 7. NanoBRET Dissociation Experiments at Room Temperature

(A) HEK293T cells transiently expressing Nanoluc-tagged receptors (RXFP1 in blue and RXFP1(ΔLDLa) in red) were incubated to equilibrium with 1 nM TamRLX before initiation of dissociation by removal of unbound TamRLX and addition of 10 μM unlabeled relaxin. Data are pooled from four to five independent experiments and fit to a two-phase decay equation. Error bars represent SEM. Mean residuals for one-phase decay fits (B and C) or two-phase decay fits (D and E) are also shown. Rate constant determinations from two-phase decay fits are provided in Table 3.

receptors resulted in TamRLX dissociation profiles that were best fit by a two-phase exponential (Figures 11B, 11D, 11E, 11G, and 11H). The fast off-rate for the ExLink receptors (0.46 ± 0.05 min^{-1} for ExLink1 and 0.47 ± 0.09 min^{-1} for ExLink2) closely matched the monophasic of rate observed for RXFP2, suggesting that the fast component relates to relaxin binding interactions with the LRRs. In addition, the percentage of fast component decreased as the linker length increased (79.01% ± 0.85% fast for ExLink1; 49.43% ± 11.8% fast for ExLink2), approaching the levels seen for RXFP1. The data suggest that the dissociation of relaxin from RXFP2 occurs in a simple, one-step fashion but that the insertion of a secondary binding site alters the kinetic profile to resemble that seen in RXFP1.

NMR Titrations of Relaxin with LDLa-Linker Proteins

We have previously designed and characterized the recombinant LDLa-linker constructs, $RXFP1_{(1-72)}$ (Sethi et al., 2016) and $RXFP2_{(1-65)}$ (Bruell et al., 2017) and investigated their interaction with relaxin using solution NMR spectroscopy and performing relaxin titrations monitored by 2D ^{1}H-^{15}N Heteronuclear Single Quantum Coherence (HSQC). For $RXFP1_{(1-72)}$, residues within the linker region (Asp51, Ala55, Tyr57, and Thr61) showed significant chemical shift differences (Figure 12A), whereas for $RXFP2_{(1-65)}$, residues within the LDLa module (Cys26, Asp30, and Glu38) and Asp43 from the N-terminal end of the linker region showed major chemical shift perturbations (Figure 12B), albeit weaker than those of $RXFP1_{(1-72)}$. By inserting the proposed relaxin-binding region from $RXFP1_{(1-72)}$ into $RXFP2_{(1-65)}$, thus creating the chimera $RXFP2_{(1-65)}$-ExLink, we were able to confirm that the interaction surface was shifted away from the LDLa module and into the extended linker as demonstrated by the significant chemical shift perturbations of linker residues Ile50, Thr60, and Ala65 (Figure 12C). Importantly, no residues within the LDLa module of $RXFP2_{(1-65)}$-ExLink show significant chemical shift differences. Fitting these differences of Ile50, Thr60, and Ala65 to a single-site binding curve shows the affinity of relaxin for $RXFP2_{(1-65)}$-ExLink is 187 ± 7 μM (compared with 330 ± 10 μM for $RXFP2_{(1-65)}$; Bruell et al., 2017;

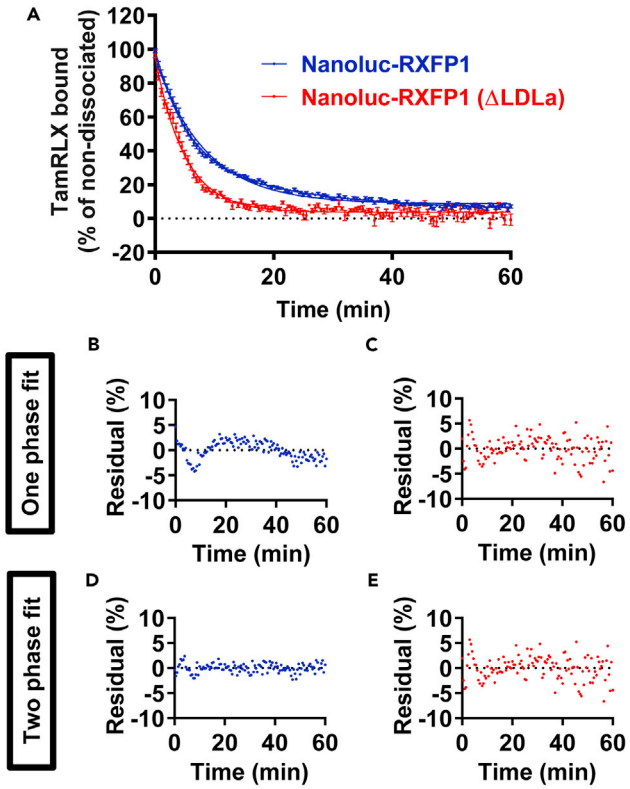

Figure 8. NanoBRET Dissociation Experiments at 37°C

(A) HEK293T cells transiently expressing Nanoluc-tagged receptors (RXFP1 in blue and RXFP1(ΔLDLa) in red) were incubated to equilibrium with 5 nM TamRLX before initiation of dissociation by injection of unlabeled relaxin to a concentration of 5 μM. Data are pooled from five independent experiments and fit to a two-phase decay equation (Nanoluc-RXFP1) or one-phase decay equation (Nanoluc-RXFP1(ΔLDLa)). Error bars represent SEM. Mean residuals for one-phase decay fits (B and D) or two-phase decay fits (C and E) are also shown. Rate constant determinations from two-phase decay fit (Nanoluc-RXFP1) or one-phase decay fit (Nanoluc-RXFP1(ΔLDLa)) are provided in Table 3.

Figure S4), suggesting a significant gain in the relaxin binding affinity for the extended RXFP2 linker. This further supports the idea that the RXFP1 linker plays a pivotal role in the binding of relaxin.

DISCUSSION

Relaxin activates RXFP1 through interactions with multiple domains in the ECD of RXFP1. However, the exact mechanism by which these domains combine to agonize the receptor has been difficult to establish. The current multi-step model of RXFP1 activation hypothesizes that a conformational rearrangement in the ECD of RXFP1 upon relaxin binding drives LDLa/linker-TMD interactions to activate the receptor. Recent NMR studies have shown that relaxin interacts with the linker domain to promote the extension of a helix within the linker (Sethi et al., 2016), and this piece of information has been key in mechanistically bridging the connection between relaxin binding (predicted to be predominantly in the LRR domain) and activation of the TMD via the LDLa-linker. These experiments, however, were performed using purified fragments of the ECD and relaxin. Indeed, the proposed multi-step mechanism is a supposition based on knowledge of the complex nature of relaxin:RXFP1 binding interactions—kinetic evidence was lacking. We therefore sought a facile and sensitive assay system in which to investigate relaxin binding kinetics in whole cells to test a single-step model (hence indirectly supporting or invalidating a multi-step model), and thus successfully established a NanoBRET-based binding technique in live HEK293T cells in a 96-well-plate-based format. Addition of tags (Nanoluc on RXFP1 N terminus and TAMRA on relaxin) was well tolerated, and NanoBRET saturation binding experiments produced TamRLX binding K_d of 0.42 ± 0.03 nM. This is consistent with published affinities from traditional fluorescence-intensity-based approaches using europium-labeled relaxin (Shabanpoor et al., 2012) or radiolabeled relaxin (Halls et al., 2005), however, with the

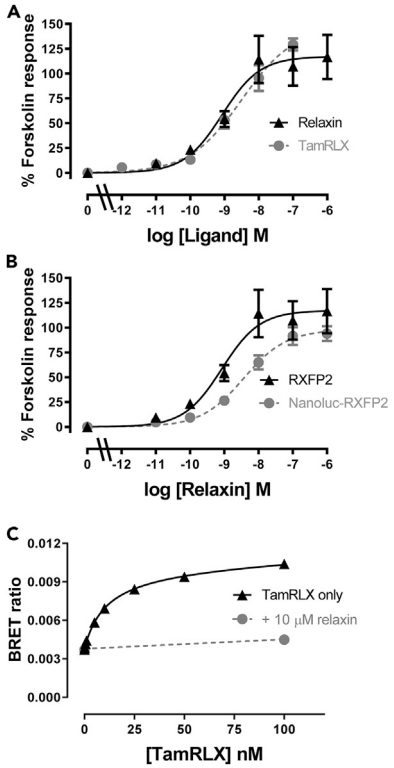

Figure 9. Characterization of TamRLX and Nanoluc-RXFP2 and NanoBRET Saturation Binding

(A) Dose-response curves of cAMP activity in HEK293T cells expressing RXFP2 when stimulated with relaxin or TamRLX. Pooled data from two to three independent experiments performed in triplicate.

(B) Dose-response curves of cAMP activity in HEK293T cells transiently expressing either RXFP2 or Nanoluc-RXFP2 and stimulated with relaxin, using cAMP reporter gene system. Pooled data from three independent experiments performed in triplicate.

(C) TamRLX saturation binding in HEK293T cells transiently expressing Nanoluc-RXFP2. Pooled data from three independent experiments performed in duplicate. All error bars (where visible) represent SEM. All K_d determinations are provided in Table 2.

notable advantage that these experiments do not require the removal of unbound labeled relaxin and have minimal non-specific signal.

It is counterintuitive that lower expression levels provided the best NanoBRET binding signal (Figure 2D); however, this can be explained by our observation that that RXFP1 (like many GPCRs) appears to accumulate significantly within intracellular compartments when overexpressed, presumably due to overwhelming the receptor trafficking machinery of the cell. As BRET is a ratiometric measurement, accumulation of intracellular receptor that cannot bind ligand would decrease the NanoBRET binding signal accordingly, hence the lowest expression (allowing the greatest proportion of receptor to traffic to the cell surface) is preferred. This should be seen as a great strength of NanoBRET measurements of ligand binding as the brightness of Nanoluc combined with the ratiometric nature of BRET means that lower levels of expression are actually preferable (resulting in less intracellular accumulation and improved signal:noise assay performance), contrasting with traditional radioligand binding assays wherein supraphysiological expression levels are often required to obtain a sufficiently strong signal.

Initially, we performed TamRLX saturation binding experiments on Nanoluc-RXFP1 constructs in which key domains had been removed or mutated. The current model of relaxin binding suggests that relaxin binds concomitantly across two sites, the LRR domain and the linker domain. The affinity of the LRR domain has been estimated to be around 1 μM, a rough calculation based on the affinity for the linker domain alone (approximately 200 μM) and for the full-length receptor (approximately 1 nM). Using NanoBRET, we measured the affinity of TamRLX to be 121 ± 5.9 nM for the LRR domain attached to a membrane anchor

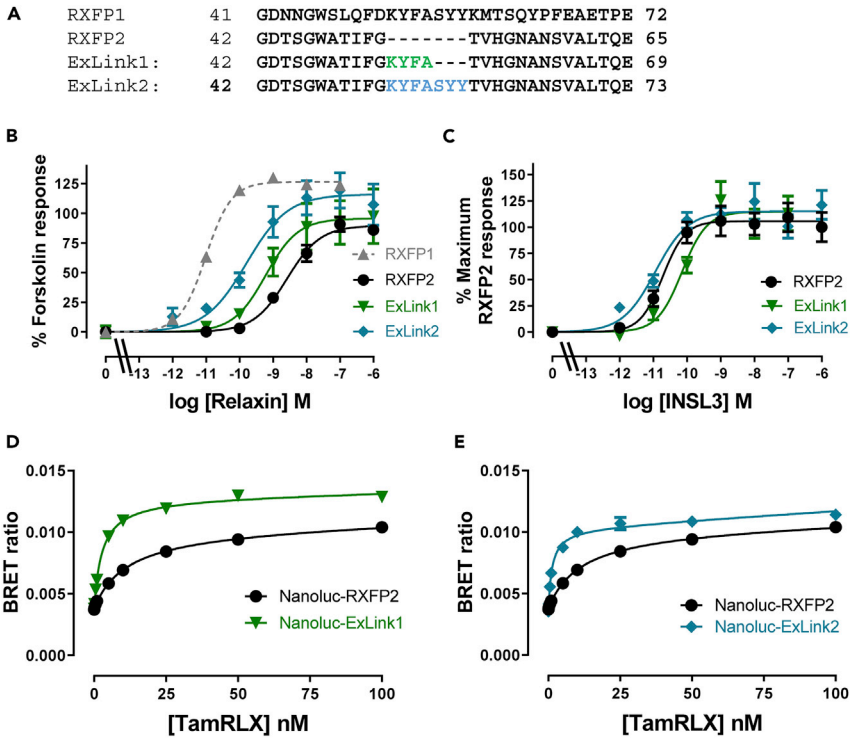

Figure 10. Comparison of Extended Linker (ExLink) Constructs with RXFP1 and RXFP2

(A) Sequence alignment of RXFP1 and RXFP2 linkers, followed by ExLink1 with inserted residues shown in green and ExLink2 with inserted residues in blue.

(B and C) cAMP activity data comparing RXFP1 and RXFP2 with ExLink constructs in response to (B) relaxin and (C) INSL3. HEK293T cells transiently expressing constructs incubated with varying concentrations of ligand. Pooled data from at least three independent experiments performed in triplicate. All E_{max} and pEC_{50} determinations are provided in Table 1.

(D and E) TamRLX saturation binding in HEK293T cells transiently expressing (D) Nanoluc-ExLink1 and (E) Nanoluc-ExLink2 compared with Nanoluc-RXFP2. Pooled data from three independent experiments performed in duplicate. All K_d determinations are provided in Table 2. All error bars (where visible) represent SEM.

(Figure 4D), or 58 ± 13 nM when attached to the RXFP1 TMD (Figure 4C). The exoloops of RXFP1 have been demonstrated to potentially comprise an additional relaxin-binding site (Diepenhorst et al., 2014; Halls et al., 2005); however, these results indicate that this site does not contribute significantly to relaxin binding affinity. Conversely, the linker domain is a significant contributor to relaxin binding affinity, as when the linker and LRR domains are present together, there is a 50- to 100-fold improvement in relaxin binding affinity compared with the LRR domain alone.

We showed that mutation of key relaxin-binding residues in LRR8 (E277Q/D279N) was sufficient to completely abolish detectable TamRLX binding and that weak binding could be restored when this mutation was applied to an ECD-only construct. This suggests that remaining known relaxin interactions within the ectodomain may be inaccessible when the LDLa/linker domains form contacts with the TMD, thus removal of the TMD might "open" the ECD to form an unnatural binding mode for relaxin. It also indicates that the LRR domain interactions are critically involved in the initial step of relaxin binding to RXFP1. Another important difference between full-length and ECD-only RXFP1 constructs was the effect of the F54A/Y58A linker domain mutation, which resulted in a 10-fold decrease in TamRLX binding affinity to the full-length receptor but did not change binding affinity for the ECD-only construct. It is difficult to explain this observation, but it again suggests that there is an unnatural binding mode for relaxin on the ECD-only construct of RXFP1.

Differences in the binding mode of full-length RXFP1 compared with ECD-only RXFP1 constructs have been noted before from observations that INSL3 (cognate peptide ligand for the related RXFP2 receptor) binds with high affinity to the ECD-only construct of RXFP1, but only with weak affinity to full-length RXFP1 (Halls

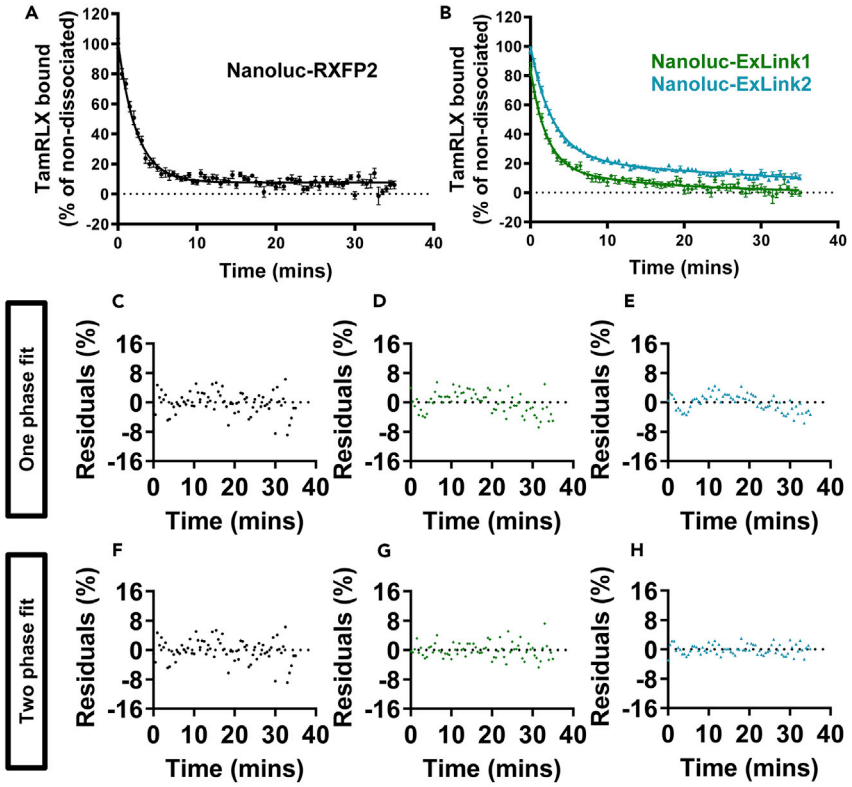

Figure 11. NanoBRET Dissociation Experiments at Room Temperature

(A and B) HEK293T cells transiently expressing Nanoluc-tagged receptors (RXFP2 in black, ExLink1 in green, and ExLink2 in teal) were incubated to equilibrium with 13 nM TamRLX before initiation of dissociation by addition of 10 μM unlabeled relaxin. Data are pooled from 4–12 independent experiments and fit to a one-phase decay equation (RXFP2) or two-phase decay equation (ExLink1 and ExLink2). Error bars represent SEM. Mean residuals for one-phase decay fits (C–E) or two-phase decay fits (F–H) are also shown. Rate constant determinations from fits are provided in Table 3.

et al., 2005; Scott et al., 2012). Representations of RXFP1 have often depicted the ECD in an "open" configuration, with the LDLa domain floating unconstrained in the extracellular space until a relaxin-binding event triggers interaction of the LDLa with the TMD. Published descriptions of the relaxin binding and LDLa activation events still allude to relaxin binding being responsible for driving the LDLa to interact with the TMD (Summers, 2017). The idea of relaxin initiating a movement of the LDLa toward the TMD comes from previous studies that suggested a low-affinity binding site for relaxin in ECL2 of the TMD (Halls et al., 2005; Diepenhorst et al., 2014). Thus the logical thought was that high-affinity relaxin binding to the LRR domain was followed by the lower affinity interactions in ECL2, thereby bringing the LDLa into contact with the TMD. This would be analogous to the general mechanism of peptide binding in Class B GPCRs, where the C terminus of the peptide ligand forms an initial complex with the ECD, followed by the N terminus of the peptide ligand interacting with the TMD to activate the receptor (Hollenstein et al., 2014). However, more recently, Sethi et al. (2016) elegantly showed interactions of the LDLa/linker with the ECL2 in the absence of relaxin, suggesting a degree of constitutive interaction. Given the current lack of published structures for RXFP1, the known interactions of the LDLa/linker with the extracellular loops in the absence of relaxin, and the observations provided here, it may be more appropriate to visualize the ECD in a perpetually "closed" configuration in which relaxin binding drives specific conformational rearrangements within the ECD allowing the LDLa-linker to activate the TMD.

An unexpected finding in saturation binding experiments was that removal of the LDLa module slightly decreased relaxin binding affinity, contrary to previous reports that relaxin binding is unaffected by LDLa removal (Scott et al., 2006; Kong et al., 2013; Hopkins et al., 2007). Interestingly, this difference was also evident in ECD-only constructs, as well as at 37°C and in HEK293 cells lacking $G_{\alpha s}$, suggesting

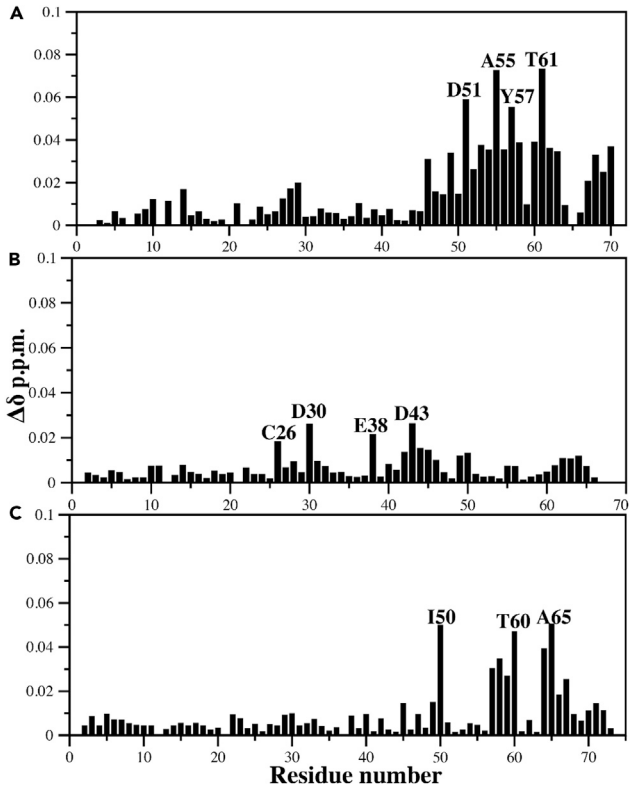

Figure 12. NMR Titrations

Plot of change in average ^{1}HN and ^{15}N chemical shifts following titration of relaxin into (A) ^{15}N-RXFP1$_{(1\text{-}72)}$, (B) ^{15}N-RXFP2$_{(1\text{-}65)}$, and (C) ^{15}N-RXFP2$_{(1\text{-}65)}$-ExLink. Residues with the greatest change are labeled above. Full HSQC spectra are shown in Figure S5.

that LDLa interactions to activate the TMD are not responsible for this subtle change. The differing results here are likely due to the increased sensitivity provided by the NanoBRET system—experimental error using more traditional techniques could obscure such subtle differences. As the LDLa domain has been shown to not have any direct binding interactions with relaxin (Sethi et al., 2016; Hopkins et al., 2007), it may be that the LDLa domain has uncharacterized interactions with relaxin-binding sites in the LRR module and/or linker domain, which modulate how relaxin interacts with these sites. Indeed, previous NMR experiments using purified LDLa/linker from RXFP2 saw heterogeneity in resonances, which were suspected to be caused by the linker domain "wrapping" back toward the N terminus of the LDLa (Bruell et al., 2017). It may be possible that the linker folds back over the LDLa module in RXFP1, and so relaxin interactions with the linker domain would be subtly affected by removal of the LDLa.

An important reason for developing the NanoBRET binding assay was to perform real-time measurements of relaxin association to and dissociation from RXFP1. Association assays followed the binding of TamRLX to Nanoluc-RXFP1 (with or without LDLa module) in real time and were analyzed based on the assumption of a single-step binding mechanism. This assumption appeared valid at first, as there was a good linear relationship between the observed rate of association (k_{obs}) and the concentration of TamRLX. This provided on- and off-rates for what would seemingly be a simple bimolecular interaction. The key interpretative aspect of these association experiments was that the K_d calculated from on- and off-rates should closely match those obtained in equilibrium saturation binding assays, provided a single-step binding mechanism is valid. However, this was not true. For Nanoluc-RXFP1, the K_d from association experiments was 1.2 nM compared with 0.42 nM in equilibrium saturation binding experiments, which, admittedly, is close enough to be considered the "same" when considering the magnitude of experimental error that is expected. However, there was an almost 10-fold difference when the LDLa was deleted (1.1 nM in equilibrium saturation binding experiments compared with 9.6 nM in association

experiments). This discrepancy leads us to reject a single-step binding mechanism in favor of the proposed multi-step mechanism.

If relaxin binding is a multi-step mechanism, why was there a linear relationship between k_{obs} versus the concentration of TamRLX? In the case of a multi-step binding/activation hypothesis, we might expect an initial diffusion-limited binding interaction between relaxin and RXFP1, followed by one or more conformational rearrangement steps, leading to a final activated relaxin-bound state of RXFP1. Such a mechanism might lead to a hyperbolic relationship between k_{obs} and TamRLX at high-enough ligand concentrations (Tummino and Copeland, 2008). Or, for example, a two-phase association profile might be encountered where one phase relates to the initial diffusion-limited ligand binding interaction and the second phase relates to the secondary rate-limited conformational rearrangement step, as has been shown in ligand association experiments with the parathyroid receptor (Castro et al., 2005) and neurokinin A receptor (Palanche et al., 2001). If a secondary conformational rearrangement step occurs with a very high rate constant (i.e., much faster than the off-rate of the initial binding interaction), then it is likely that much higher ligand concentrations would be required to observe a two-phase association profile or non-linearity of the k_{obs} versus TamRLX concentration dependency.

We observed a two-phase dissociation profile of TamRLX from Nanoluc-RXFP1 (Figures 7 and 9), which suggests two relaxin-bound states of RXFP1 and further supports a multi-step binding mechanism. For canonical GPCRs in which ligand binding is directly coupled to G protein activation, this observation might be explained as being caused by G protein-coupled and G protein-uncoupled states of the receptor, because G protein coupling is often associated with an increase in the affinity of bound ligand. However, this explanation is not sufficient in this case as removal of the LDLa module (which activates the TMD) also showed two-phase dissociation profiles. In addition, saturation binding experiments in HEK293 cells lacking $G_{\alpha s}$, the primary G protein to which RXFP1 is coupled in HEK cells, did not show any significant difference in relaxin binding affinity, and previous studies have found no change in relaxin binding affinity in membrane preparations in the presence of the non-hydrolysable GTP analogs, Gpp(NH)p and GTPγS (Scott et al., 2006). Another alternative explanation for a two-phase TamRLX dissociation relates to possible homodimerization of RXFP1 (Svendsen et al., 2008), or differing localization of the receptor within the cell (for example, intracellular pools of receptor, receptor clustering within different membrane microdomains, or receptor internalization), providing a framework by which two relaxin-binding sites might exist with two slightly different affinities. These explanations also fall short for three reasons. First, the saturation binding curves for RXFP1 fit very well to a one-site equation. There is no evidence of a biphasic saturation profile to indicate the presence of two distinct relaxin-binding sites that may be concomitantly occupied. Second, association experiments clearly showed a monophasic association profile at the concentrations tested. The existence and occupancy of two distinct binding sites at the relaxin concentrations used should in theory produce a more complex association profile. Third, RXFP1 has been shown to lack arrestin recruitment and does not appear to appreciably internalize upon receptor activation (Callander et al., 2009; Kern and Bryant-Greenwood, 2008). Thus the evidence suggests relaxin binding to a single site with a multi-step mechanism rather than simply binding to two distinct sites, which is concordant with the current proposed model for RXFP1 binding/activation (Sethi et al., 2016).

Supporting this idea is our observation that RXFP2, which does not contain a relaxin-linker-binding site, does not follow a similar two-phase profile of relaxin dissociation, but shows a clear one-phase exponential decay. Importantly, insertion of RXFP1 linker residues that interact with relaxin clearly increases relaxin affinity and activity at the chimeric receptors, whereas TamRLX dissociation assays highlight the reinstatement of a two-phase dissociation profile. These data in conjunction with NMR studies, which show binding of relaxin to the introduced linker sequence, clearly demonstrate the key role of the linker region in relaxin affinity and the multi-step binding mechanism. However, it should be emphasized that the relaxin:RXFP1 binding interaction does not appear to be a strictly sequential binding process between the two sites (i.e., LRR binding followed by linker binding), but rather a concomitant binding interaction over both LRR/linker domains followed by conformational changes allowing LDLa/linker activation of the TMD. The linker domain is hence involved in all steps of this process, and this is seen most clearly in our observation that the RXFP1(F54A/Y58A) mutation in the linker-binding site in RXFP1 also showed a clear two-phase dissociation of TamRLX (Figure S3) in which both rates were increased compared with wild-type.

Overall, these studies have provided valuable insight into the mechanism by which relaxin binds to RXFP1 and RXFP2, and NanoBRET represents a valuable tool by which these interactions may be investigated in future. TamRLX association and dissociation experiments provided support for a more complex binding

mode than a simple one-step bimolecular interaction, fitting with a hypothesized multi-step model of relaxin binding/activation. In addition, we found that the LDLa module does subtly influence how relaxin binds to the receptor, and that it appears to have a role in stabilizing a higher-affinity relaxin-bound state of the ECD. This may be related to LDLa having interactions with the LRR and/or linker domains, and this possibility should be investigated in the future.

Limitations of the Study

The requirement of a NanoBRET ligand binding assay is the introduction of tags (Nanoluc on the receptor and Tamra on relaxin), which may affect how relaxin binds to RXFP1. Indeed, both Nluc-RXFP1 and TamRLX showed very small perturbations in their respective abilities to be activated by relaxin, and to activate the untagged receptor (Figures 2A and 2B). The exact rates of relaxin binding presented here will therefore differ slightly from the "true" rates in an untagged system. Importantly, however, this does not affect interpretations about the relative contributions of each receptor binding domain to the overall relaxin:RXFP1 binding mode (for example, a 50- to 100-fold decrease in relaxin binding affinity when the linker and LDLa were removed from RXFP1). Furthermore, we are confident that the observed biphasic dissociation profile of TamRLX from Nluc-RXFP1 truly reflects the interpretation of two relaxin-bound RXFP1 states in which the linker domain plays an important role, as opposed to simply being an artifact of the NanoBRET system. This is most clearly demonstrated by the monophasic dissociation profile of TamRLX from Nluc-RXFP2, which could be converted to a biphasic dissociation profile by introduction of the RXFP1 linker domain. Hence, although the NanoBRET tags used here may influence the exact rates of binding, we believe that the interpretations drawn are valid.

METHODS

All methods can be found in the accompanying Transparent Methods supplemental file.

DATA AND SOFTWARE AVAILABILITY

The chemical shift assignments for RXFP2(1-65)- ExLink have been deposited in the BioMagResBank (http://www.bmrb.wisc.edu) under the accession number 27601.

SUPPLEMENTAL INFORMATION

Supplemental Information includes Transparent Methods and five figures and can be found with this article online at https://doi.org/10.1016/j.isci.2018.12.004.

ACKNOWLEDGMENTS

This research was supported by National Health and Medical Research Council of Australia project grants 1100676 and 1043750 (R.A.D.B., P.R.G., and D.J.S.) and the Victorian Government Operational Infrastructure Support Program. A.I. was funded by Japan Agency for Medical Research and Development (AMED) grant number JP17gm5910013 and Japan Society for the Promotion of Science (JSPS) KAKENHI grant number 17K08264. R.A.D.B. is supported by an NHMRC Research Fellowship, and D.J.S. is supported by an NHMRC Dementia Fellowship. The authors thank Tania Ferraro and Sharon Layfield for technical assistance.

AUTHOR CONTRIBUTIONS

B.L.H., S.B., and A.S. conducted the experiments. B.L.H., S.B., A.S., P.R.G., D.J.S., and R.A.D.B. conceived experiments and analyzed the data. M.A.H. synthesized TamRLX, A.I. provided HEK293A $\Delta G_{\alpha s}$ knockout cells, and M.J.L. assisted with design and analysis of kinetic experiments. B.J.H., S.B., A.S., P.R.G., D.J.S., and R.A.D.B. wrote the manuscript. All authors have given approval to the final version of the manuscript.

DECLARATION OF INTERESTS

The authors declare that they have no conflicts of interest with the contents of this article.

Received: October 3, 2018
Revised: November 20, 2018
Accepted: December 5, 2018
Published: January 25, 2019

REFERENCES

Bathgate, R.A., Ivell, R., Sanborn, B.M., Sherwood, O.D., and Summers, R.J. (2006). International Union of Pharmacology LVII: recommendations for the nomenclature of receptors for relaxin family peptides. Pharmacol. Rev. *58*, 7.

Bruell, S., Kong, R.C., Petrie, E.J., Hoare, B., Wade, J.D., Scott, D.J., Gooley, P.R., and Bathgate, R.A. (2013). Chimeric RXFP1 and RXFP2 receptors highlight the similar mechanism of activation utilizing their N-terminal low-density lipoprotein class A modules. Front. Endocrinol. *4*, 171.

Bruell, S., Sethi, A., Smith, N., Scott, D.J., Hossain, M.A., Wu, Q.-P., Guo, Z.-Y., Petrie, E.J., Gooley, P.R., and Bathgate, R.A.D. (2017). Distinct activation modes of the Relaxin Family Peptide Receptor 2 in response to insulin-like peptide 3 and relaxin. Sci. Rep. *7*, 3294.

Bullesbach, E.E., and Schwabe, C. (2005). The trap-like relaxin-binding site of the leucine-rich G-protein-coupled receptor 7. J. Biol. Chem. *280*, 14051–14056.

Callander, G.E., Thomas, W.G., and Bathgate, R.A. (2009). Prolonged RXFP1 and RXFP2 signaling can be explained by poor internalization and a lack of β-arrestin recruitment. Am. J. Physiol. Cell Physiol. *296*, C1058–C1066.

Castro, M., Nikolaev, V.O., Palm, D., Lohse, M.J., and Vilardaga, J.-P. (2005). Turn-on switch in parathyroid hormone receptor by a two-step parathyroid hormone binding mechanism. Proc. Natl. Acad. Sci. U S A *102*, 16084–16089.

Chen, C.Z., Southall, N., Xiao, J., Marugan, J.J., Ferrer, M., Hu, X., Jones, R.E., Feng, S., Agoulnik, I.U., and Zheng, W. (2013). Identification of small-molecule agonists of human relaxin family receptor 1 (RXFP1) by using a homogenous cell-based cAMP assay. J. Biomol. Screen. *18*, 670–677.

Christiansen, E., Hudson, B.D., Hansen, A.H., Milligan, G., and Ulven, T. (2016). Development and characterization of a potent free fatty acid receptor 1 (FFA1) fluorescent tracer. J. Med. Chem. *59*, 4849–4858.

Diepenhorst, N.A., Petrie, E.J., Chen, C.Z., Wang, A., Hossain, M.A., Bathgate, R.A., and Gooley, P.R. (2014). Investigation of interactions at the extracellular loops of the relaxin family peptide receptor 1 (RXFP1). J. Biol. Chem. *289*, 34938–34952.

England, C.G., Ehlerding, E.B., and Cai, W. (2016). NanoLuc: a small luciferase is brightening up the field of bioluminescence. Bioconjug. Chem. *27*, 1175–1187.

Fevold, H., Hisaw, F.L., and Meyer, R. (1930). The relaxative hormone of the corpus luteum. Its purification and concentration. J. Am. Chem. Soc. *52*, 3340–3348.

Hall, M.P., Unch, J., Binkowski, B.F., Valley, M.P., Butler, B.L., Wood, M.G., Otto, P., Zimmerman, K., Vidugiris, G., and Machleidt, T. (2012). Engineered luciferase reporter from a deep sea shrimp utilizing a novel imidazopyrazinone substrate. ACS Chem. Biol. *7*, 1848.

Halls, M.L., Bond, C.P., Sudo, S., Kumagai, J., Ferraro, T., Layfield, S., Bathgate, R.A., and Summers, R.J. (2005). Multiple binding sites revealed by interaction of relaxin family peptides with native and chimeric relaxin family peptide receptors 1 and 2 (LGR7 and LGR8). J. Pharmacol. Exp. Ther. *313*, 677–687.

Hansen, A.H., Sergeev, E., Pandey, S.K., Hudson, B.D., Christiansen, E., Milligan, G., and Ulven, T. (2017). Development and characterization of a fluorescent tracer for the free fatty acid receptor 2 (FFA2/GPR43). J. Med. Chem. *60*, 5638–5645.

Hollenstein, K., De Graaf, C., Bortolato, A., Wang, M.-W., Marshall, F.H., and Stevens, R.C. (2014). Insights into the structure of class B GPCRs. Trends Pharmacol. Sci. *35*, 12–22.

Hopkins, E.J., Layfield, S., Ferraro, T., Bathgate, R.A., and Gooley, P.R. (2007). The NMR solution structure of the relaxin (RXFP1) receptor lipoprotein receptor class A module and identification of key residues in the N-terminal region of the module that mediate receptor activation. J. Biol. Chem. *282*, 4172–4184.

Hsu, S.Y., Nakabayashi, K., Nishi, S., Kumagai, J., Kudo, M., Sherwood, O.D., and Hsueh, A.J. (2002). Activation of orphan receptors by the hormone relaxin. Science *295*, 671–674.

Huang, Z., Myhr, C., Bathgate, R.A., Ho, B.A., Bueno, A., Hu, X., Xiao, J., Southall, N., Barnaeva, E., and Agoulnik, I.U. (2015). Activation of relaxin family receptor 1 from different mammalian species by relaxin peptide and small-molecule agonist ML290. Front. Endocrinol. *6*, 128.

Kern, A.S., and Bryant-Greenwood, G.D. (2008). Characterization of relaxin receptor (RXFP1) desensitization and internalization in primary human decidual cells and RXFP1-transfected HEK293 cells. Endocrinology *150*, 2419–2428.

Kilpatrick, L., Robers, M., Friedman-Ohana, R., Zimmerman, K., Woolard, J., and Hill, S. (2017a). Use of bioluminescence resonance energy transfer (BRET) and fluorescent vascular endothelial growth factor (VEGF) isoforms to characterize the molecular pharmacology of neuropilin-1 receptors in living HEK293 cells. FASEB J. *31*, lb551.

Kilpatrick, L.E., Friedman-Ohana, R., Alcobia, D.C., Riching, K., Peach, C.J., Wheal, A.J., Briddon, S.J., Robers, M.B., Zimmerman, K., and Machleidt, T. (2017b). Real-time analysis of the binding of fluorescent VEGF 165 a to VEGFR2 in living cells: effect of receptor tyrosine kinase inhibitors and fate of internalized agonist-receptor complexes. Biochem. Pharmacol. *136*, 62–75.

Kocan, M., Sarwar, M., Ang, S.Y., Xiao, J., Marugan, J.J., Hossain, M.A., Wang, C., Hutchinson, D.S., Samuel, C.S., and Agoulnik, A.I. (2017). ML290 is a biased allosteric agonist at the relaxin receptor RXFP1. Sci. Rep. *7*, 2968.

Kong, R.C., Petrie, E.J., Mohanty, B., Ling, J., Lee, J.C., Gooley, P.R., and Bathgate, R.A. (2013). The relaxin receptor (RXFP1) utilizes hydrophobic moieties on a signaling surface of its N-terminal low density lipoprotein class A module to mediate receptor activation. J. Biol. Chem. *288*, 28138–28151.

Lekgabe, E.D., Kiriazis, H., Zhao, C., Xu, Q., Moore, X.L., Su, Y., Bathgate, R.A., Du, X.-J., and Samuel, C.S. (2005). Relaxin reverses cardiac and renal fibrosis in spontaneously hypertensive rats. Hypertension *46*, 412–418.

Lu, H., and Tonge, P.J. (2010). Drug–target residence time: critical information for lead optimization. Curr. Opin. Chem. Biol. *14*, 467–474.

Machleidt, T., Woodroofe, C.C., Schwinn, M.K., Méndez, J., Robers, M.B., Zimmerman, K., Otto, P., Daniels, D.L., Kirkland, T.A., and Wood, K.V. (2015). NanoBRET–a novel BRET platform for the analysis of protein–protein interactions. ACS Chem. Biol. *10*, 1797–1804.

Palanche, T., Ilien, B., Zoffmann, S., Reck, M.-P., Bucher, B., Edelstein, S.J., and Galzi, J.-L. (2001). The neurokininA receptor activates calcium and cAMP responses through distinct conformational states. J. Biol. Chem. *276*, 34853–34861.

Peach, C., Kilpatrick, L., Robers, M., Ohana-Friedman, R., Woolard, J., and Hill, S. (2017). Measurement of the binding of fluorescent variants of VEGF165a, VEGF165b and VEGF121a to VEGFR2 using NanoBRET in HEK293 cells. FASEB J. *31*, lb537.

Samuel, C.S., Du, X.-J., Bathgate, R.A., and Summers, R.J. (2006). 'Relaxin'the stiffened heart and arteries: the therapeutic potential for relaxin in the treatment of cardiovascular disease. Pharmacol. Ther. *112*, 529–552.

Scott, D.J., Layfield, S., Yan, Y., Sudo, S., Hsueh, A.J., Tregear, G.W., and Bathgate, R.A. (2006). Characterization of novel splice variants of LGR7 and LGR8 reveals that receptor signaling is mediated by their unique low density lipoprotein class A modules. J. Biol. Chem. *281*, 34942–34954.

Scott, D.J., Rosengren, K.J., and Bathgate, R.A.D. (2012). The different ligand-binding modes of relaxin family peptide receptors RXFP1 and RXFP2. Mol. Endocrinol. *26*, 1896–1906.

Scott, D.J., Tregear, G.W., and Bathgate, R.A. (2009). Modeling the primary hormone-binding site of RXFP1 and RXFP2. Ann. N. Y. Acad. Sci. *1160*, 74–77.

Sethi, A., Bruell, S., Patil, N., Hossain, M.A., Scott, D.J., Petrie, E.J., Bathgate, R.A., and Gooley, P.R. (2016). The complex binding mode of the peptide hormone H2 relaxin to its receptor RXFP1. Nat. Commun. *7*, 11344.

Shabanpoor, F., Bathgate, R.A., Belgi, A., Chan, L.J., Nair, V.B., Wade, J.D., and Hossain, M.A. (2012). Site-specific conjugation of a lanthanide chelator and its effects on the chemical synthesis and receptor binding affinity of human relaxin-2 hormone. Biochem. Biophys. Res. Commun. *420*, 253–256.

Soave, M., Stoddart, L.A., Brown, A., Woolard, J., and Hill, S.J. (2016). Use of a new proximity assay (NanoBRET) to investigate the ligand-binding characteristics of three fluorescent ligands to the human β1-adrenoceptor expressed in HEK-293 cells. Pharmacol. Res. Perspect. *4*, e00250.

Stallaert, W., Van Der Westhuizen, E.T., Schonegge, A.M., Plouffe, B., Hogue, M., Lukashova, V., Inoue, A., Ishida, S., Aoki, J., Le Gouill, C., and Bouvier, M. (2017). Purinergic receptor transactivation by the beta2-adrenergic receptor increases intracellular Ca(2+) in nonexcitable cells. Mol. Pharmacol. *91*, 533–544.

Stoddart, L.A., Johnstone, E.K., Wheal, A.J., Goulding, J., Robers, M.B., Machleidt, T., Wood, K.V., Hill, S.J., and Pfleger, K.D. (2015). Application of BRET to monitor ligand binding to GPCRs. Nat. Methods *12*, 661–663.

Stoddart, L.A., Kilpatrick, L.E., and Hill, S.J. (2017). NanoBRET approaches to study ligand binding to GPCRs and RTKs. Trends Pharmacol. Sci. *39*, 136–147.

Stoddart, L.A., White, C.W., Nguyen, K., Hill, S.J., and Pfleger, K.D. (2016). Fluorescence-and bioluminescence-based approaches to study GPCR ligand binding. Br. J. Pharmacol. *173*, 3028–3037.

Summers, R. (2017). Recent progress in the understanding of relaxin family peptides and their receptors. Br. J. Pharmacol. *174*, 915–920.

Svendsen, A.M., Zalesko, A., Konig, J., Vrecl, M., Heding, A., Kristensen, J.B., Wade, J.D., Bathgate, R.A., De Meyts, P., and Nohr, J. (2008). Negative cooperativity in H2 relaxin binding to a dimericrelaxin family peptide receptor 1. Mol. Cell. Endocrinol. *296*, 10–17.

Swinney, D.C., Beavis, P., Chuang, K.T., Zheng, Y., Lee, I., Gee, P., Deval, J., Rotstein, D.M., Dioszegi, M., and Ravendran, P. (2014). A study of the molecular mechanism of binding kinetics and long residence times of human CCR5 receptor small molecule allosteric ligands. Br. J. Pharmacol. *171*, 3364–3375.

Tan, Y., Wade, J., Tregear, G., and Summers, R. (1999). Quantitative autoradiographic studies of relaxin binding in rat atria, uterus and cerebral cortex: characterization and effects of oestrogen treatment. Br. J. Pharmacol. *127*, 91–98.

Teerlink, J.R., Cotter, G., Davison, B.A., Felker, G.M., Filippatos, G., Greenberg, B.H., Ponikowski, P., Unemori, E., Voors, A.A., and Adams, K.F. (2013). Serelaxin, recombinant human relaxin-2, for treatment of acute heart failure (RELAX-AHF): a randomised, placebo-controlled trial. Lancet *381*, 29–39.

Tummino, P.J., and Copeland, R.A. (2008). Residence time of receptor– ligand complexes and its effect on biological function. Biochemistry *47*, 5481–5492.

Wang, J.-H., Shao, X.-X., Hu, M.-J., Wei, D., Liu, Y.-L., Xu, Z.-G., and Guo, Z.-Y. (2017). A novel BRET-based binding assay for interaction studies of relaxin family peptide receptor 3 with its ligands. Amino Acids *49*, 895–903.

Xiao, J., Huang, Z., Chen, C.Z., Agoulnik, I.U., Southall, N., Hu, X., Jones, R.E., Ferrer, M., Zheng, W., and Agoulnik, A.I. (2013). Identification and optimization of small-molecule agonists of the human relaxin hormone receptor RXFP1. Nat. Commun. *4*, 1953.

ISCI, Volume *11*

Supplemental Information

Multi-Component Mechanism of H2 Relaxin Binding to RXFP1 through NanoBRET Kinetic Analysis

Bradley L. Hoare, Shoni Bruell, Ashish Sethi, Paul R. Gooley, Michael J. Lew, Mohammed A. Hossain, Asuka Inoue, Daniel J. Scott, and Ross A.D. Bathgate

Supplemental information. Hoare et al.

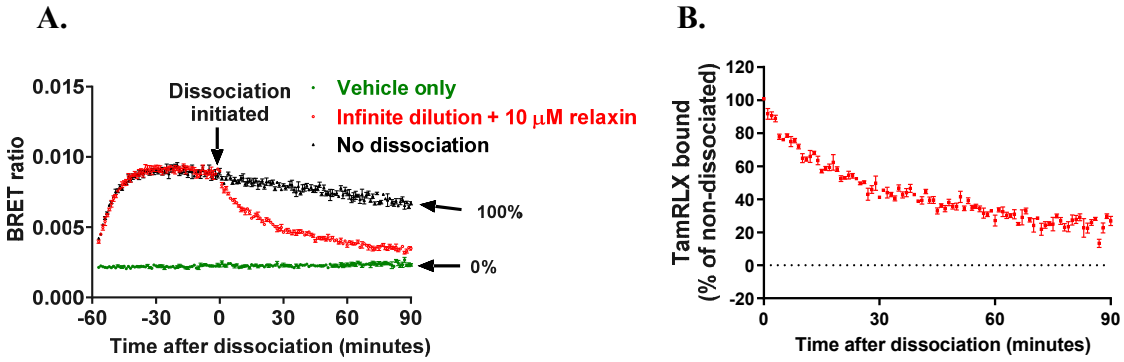

Figure S1. Related to Figures 7, 8 and 11. Raw BRET ratios from a single TamRLX dissociation experiment at room temperature. (A) HEK293T cells expressing Nanoluc-RXFP1 were incubated to equilibrium with 1 nM TamRLX before initiation of dissociation by removal of unbound TamRLX and addition of 10 μM unlabelled relaxin. **(B)** Raw BRET ratios were normalised such that vehicle only (green) was 0%, no dissociation (black) was 100%, to provide the actual dissociation profile in red. Error bars represent SEM

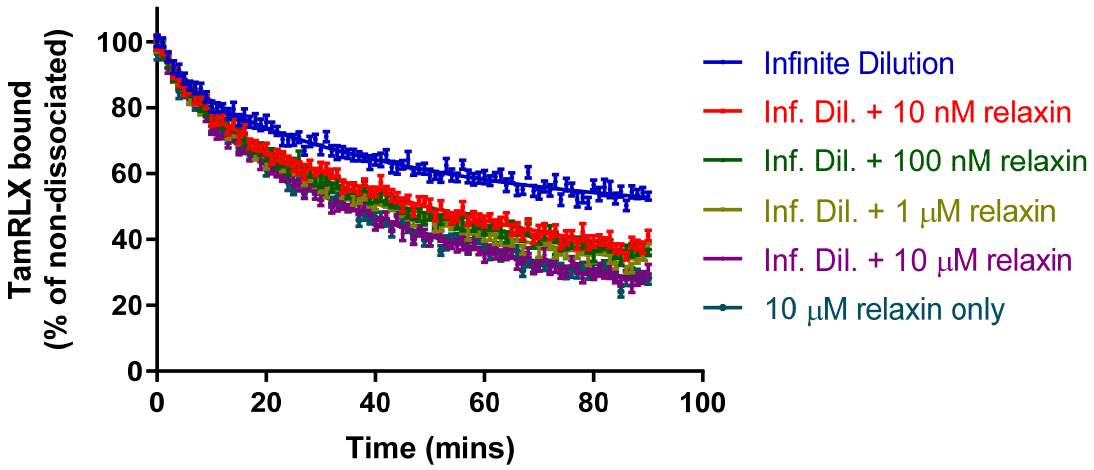

	Plateau (%)		$k_{off(FAST)}$		$k_{off(SLOW)}$		% Fast	
	Mean	SEM	Mean	SEM	Mean	SEM	Mean	SEM
Infinite Dilution	46.670	2.774	0.177	0.062	0.021	0.004	25.350	4.831
Inf. Dil. + 10 nM relaxin	23.850	5.184	0.136	0.042	0.017	0.004	22.240	4.019
Inf. Dil. + 100 nM relaxin	26.940	3.050	0.145	0.060	0.021	0.004	17.690	5.309
Inf. Dil. + 1 μM relaxin	23.430	3.313	0.141	0.047	0.020	0.003	20.070	4.687
Inf. Dil. + 10 μM relaxin	17.880	2.783	0.155	0.050	0.021	0.003	18.580	4.059
10μM relaxin only	15.230	6.250	0.104	0.049	0.018	0.006	21.140	9.590

Figure S2. Related to Figure 7: Comparison of different means of initiating TamRLX dissociation. HEK293T cells expressing Nanoluc-RXFP1 were incubated to equilibrium with 1 nM TamRLX before initiation of dissociation by removal of unbound TamRLX and addition of varying concentrations of unlabelled relaxin, or by addition of 10 μM unlabelled relaxin only (without removal of unbound TamRLX). Pooled data from 4 to 5 independent experiments performed in triplicate and in parallel; error bars represent SEM. Data fit to a biphasic exponential decay function in Graphpad prism with no constraints on plateau component, and outputs are presented in the accompanying table. Note that there is no significant difference between off-rates (fast or slow), nor in the percent of the fast component. Rather, only the plateau component appears to decrease with the addition of unlabelled competing relaxin.

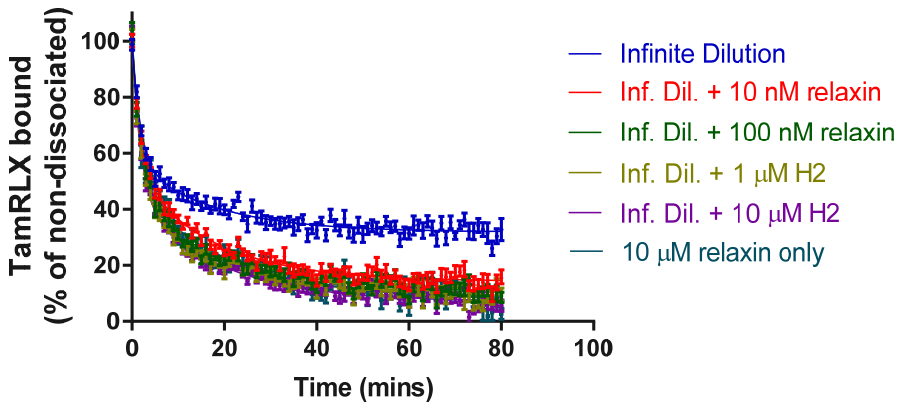

	Plateau (%)		$k_{off(FAST)}$		$k_{off(SLOW)}$		% Fast	
	Mean	SEM	Mean	SEM	Mean	SEM	Mean	SEM
Infinite Dilution	31.820	0.6169	0.5572	0.08398	0.05722	0.009025	63.11	3.936
Inf. Dil. + 10 nM relaxin	14.250	0.5157	0.5111	0.06133	0.05833	0.005146	53.95	2.946
Inf. Dil. + 100 nM relaxin	10.140	0.7551	0.4109	0.03685	0.04584	0.005875	65.53	2.543
Inf. Dil. + 1 μM relaxin	8.802	0.6376	0.4771	0.04274	0.04988	0.005558	64.58	2.398
Inf. Dil. + 10 μM relaxin	7.041	0.5482	0.5528	0.05267	0.05562	0.004977	60.27	2.355
10 μM relaxin only	7.917	0.9609	0.5203	0.08111	0.05022	0.006567	56.00	3.507

Figure S3. Related to Figure 7: Two-phase dissociation of TamRLX from Nluc-RXFP1(F54A/Y58A). HEK293T cells expressing Nanoluc-RXFP1(F54A/Y58A) were incubated to equilibrium with 10 nM TamRLX before initiation of dissociation by removal of unbound TamRLX and addition of varying concentrations of unlabelled relaxin, or by addition of 10 μM unlabelled relaxin only (without removal of unbound TamRLX). Pooled data from 4 to 5 independent experiments performed in triplicate and in parallel; error bars represent SEM. Data fit to a biphasic exponential decay function in Graphpad prism with no constraints on plateau component, and outputs are presented in the accompanying table.

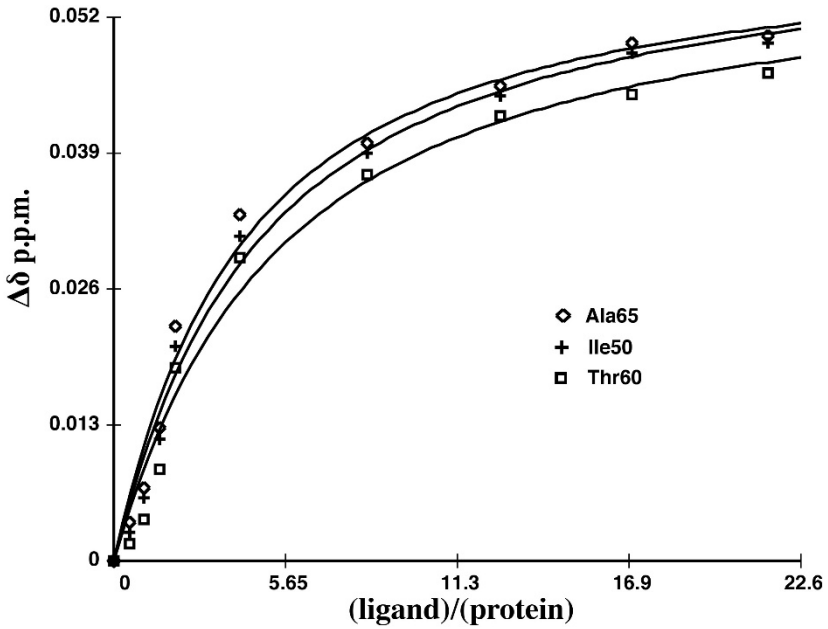

Figure S4. Related to Figure 12. Saturation curves from titration of relaxin into RXFP2$_{(1-65)}$-ExLink. K_d values were extracted from curves of chemical shift movement of residues Ile50 (crosses), Thr60 (squares) and Ala65 (diamonds).

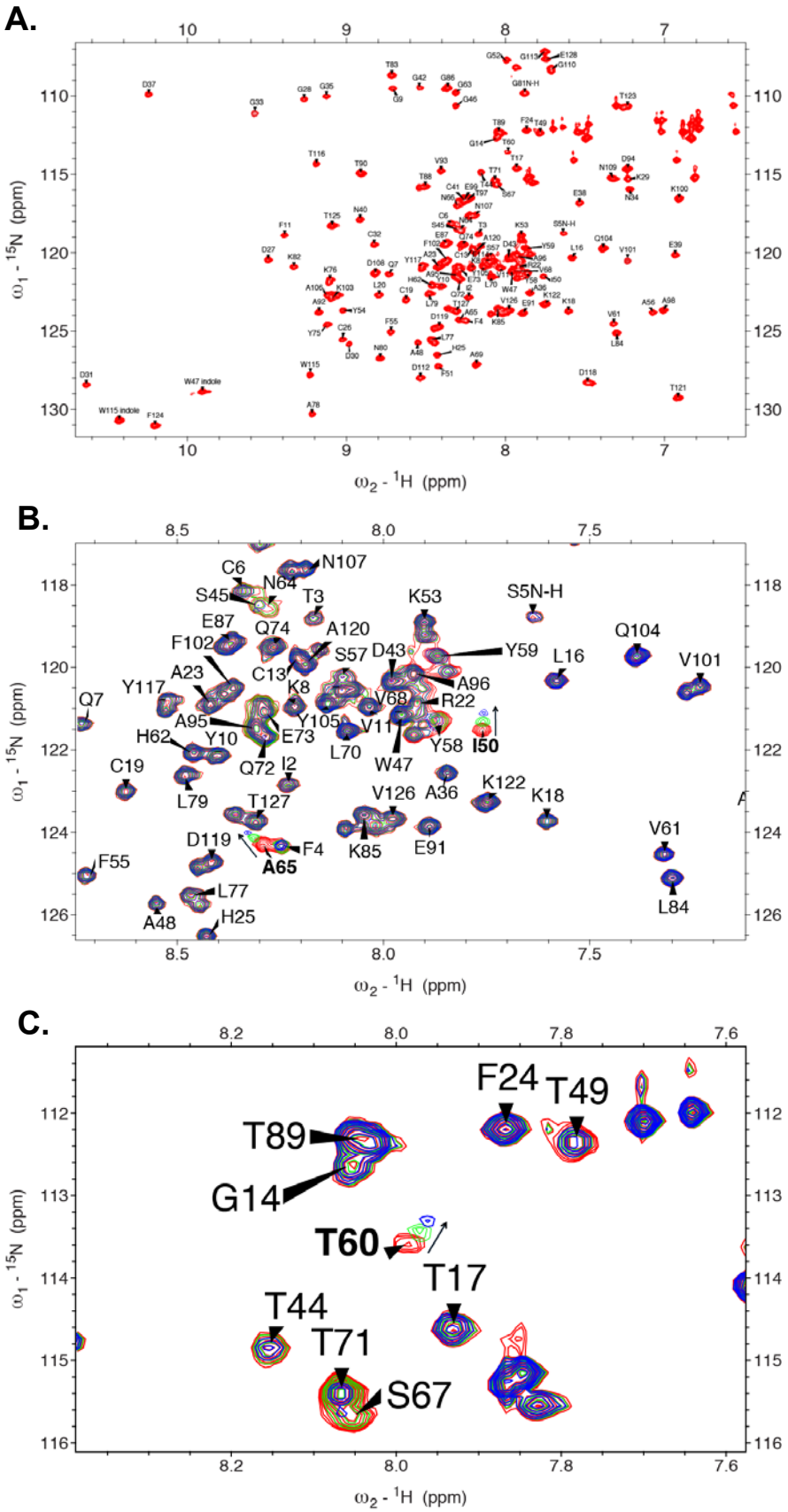

Figure S5. Related to Figure 12. (A) Full ^{1}H, ^{15}N HSQC spectrum of RXFP2$_{(1\text{-}65)}$ExLink with residue assignments. Unassigned resonances in the upper right corner belong to Asn and Gln sidechains. Residues I2 to E73 correspond to the LDLa-linker while residues Q74 to E128 belong to the GB1 tag. **(B)** and **(C)**: Representative regions of the ^{1}H, ^{15}N HSQC spectrum showing chemical shift dependence on titration with H2 relaxin (green 500 μM and blue 1 mM H2 relaxin).

Supplemental information – ORF amino acid sequences for Nanoluc-RXFP1 and Nanoluc-RXFP2 constructs used in this study, inserted in pcDNA3.1/Zeo plasmid, as well as His_6-GB1-$RXFP2_{(1-65)}$-ExLink protein construct, inserted in pET15 plasmid**.**

Bovine prolactin signal peptide

FLAG epitope tag

Nanoluc

LDLa domain

Linker domain

Leucine rich repeat domain

Transmembrane domain/C-terminus

CD8 membrane anchor (including V5 epitope, 6X His, thrombin cleavage site)

GB1 solubility tag

>Nanoluc-RXFP1

MDSKGSSQKGSRLLLLLVVSNLLLCQGVVSDYKDDDDEFGSVFTLEDFVGDWRQTAGYNLDQVLEQGGVSSLFQNLGVSVTPIQRIVL
SGENGLKIDIHVIIPYEGLSGDQMGQIEKIFKVVYPVDDHHFKVILHYGTLVIDGVTPNMIDYFGRPYEGIAVFDGKKITVTGTLWNG
NKIIDERLINPDGSLLFRVTINGVTGWRLCERILAKLEFQDVKCSLGYFPCGNITKCLPQLLHCNGVDDCGNQADEDNCGDNNGWSLQ
FDKYFASYYKMTSQYPFEAETPECLVGSVPVQCLCQGLELDCDETNLRAVPSVSSNVTAMSLQWNLIRKLPPDCFKNYHDLQKLYLQN
NKITSISIYAFRGLNSLTKLYLSHNRITFLKPGVFEDLHRLEWLIIEDNHLSRISPPTFYGLNSLILLVLMNNVLTRLPDKPLCQHMP
RLHWLDLEGNHIHNLRNLTFISCSNLTVLVMRKNKINHLNENTFAPLQKLDELDLGSNKIENLPPLIFKDLKELSQLNLSYNPIQKIQ
ANQFDYLVKLKSLSLEGIEISNIQQRMFRPLMNLSHIYFKKFQYCGYAPHVRSCKPNTDGISSLENLLASIIQRVFVWVVSAVTCFGN
IFVICMRPYIRSENKLYAMSIISLCCADCLMGIYLFVIGGFDLKFRGEYNKHAQLWMESTHCQLVGSLAILSTEVSVLLLTFLTLEKY
ICIVYPFRCVRPGKCRTITVLILIWITGFIVAFIPLSNKEFFKNYYGTNGVCFPLHSEDTESIGAQIYSVAIFLGINLAAFIIIVFSY
GSMFYSVHQSAITATEIRNQVKKEMILAKRFFFIVFTDALCWIPIFVVKFLSLLQVEIPGTITSWVVIFILPINSALNPILYTLTTRP
FKEMIHRFWYNYRQRKSMDSKGQKTYAPSFIWVEMWPLQEMPPELMKPDLFTYPCEMSLISQSTRLNSYS*

>Nanoluc-RXFP1(ΔLDLa)

MDSKGSSQKGSRLLLLLVVSNLLLCQGVVSDYKDDDDVDGSVFTLEDFVGDWRQTAGYNLDQVLEQGGVSSLFQNLGVSVTPIQRIVL
SGENGLKIDIHVIIPYEGLSGDQMGQIEKIFKVVYPVDDHHFKVILHYGTLVIDGVTPNMIDYFGRPYEGIAVFDGKKITVTGTLWNG
NKIIDERLINPDGSLLFRVTINGVTGWRLCERILAGSGDNNGWSLQFDKYFASYYKMTSQYPFEAETPECLVGSVPVQCLCQGLELDC
DETNLRAVPSVSSNVTAMSLQWNLIRKLPPDCFKNYHDLQKLYLQNNKITSISIYAFRGLNSLTKLYLSHNRITFLKPGVFEDLHRLE
WLIIEDNHLSRISPPTFYGLNSLILLVLMNNVLTRLPDKPLCQHMPRLHWLDLEGNHIHNLRNLTFISCSNLTVLVMRKNKINHLNEN
TFAPLQKLDELDLGSNKIENLPPLIFKDLKELSQLNLSYNPIQKIQANQFDYLVKLKSLSLEGIEISNIQQRMFRPLMNLSHIYFKKF
QYCGYAPHVRSCKPNTDGISSLENLLASIIQRVFVWVVSAVTCFGNIFVICMRPYIRSENKLYAMSIISLCCADCLMGIYLFVIGGFD
LKFRGEYNKHAQLWMESTHCQLVGSLAILSTEVSVLLLTFLTLEKYICIVYPFRCVRPGKCRTITVLILIWITGFIVAFIPLSNKEFF
KNYYGTNGVCFPLHSEDTESIGAQIYSVAIFLGINLAAFIIIVFSYGSMFYSVHQSAITATEIRNQVKKEMILAKRFFFIVFTDALCW
IPIFVVKFLSLLQVEIPGTITSWVVIFILPINSALNPILYTLTTRPFKEMIHRFWYNYRQRKSMDSKGQKTYAPSFIWVEMWPLQEMP
PELMKPDLFTYPCEMSLISQSTRLNSYSAS*

>Nanoluc-RXFP1(ΔLDLa/ΔLinker)

MDSKGSSQKGSRLLLLLVVSNLLLCQGVVSDYKDDDDVDGSVFTLEDFVGDWRQTAGYNLDQVLEQGGVSSLFQNLGVSVTPIQRIVL
SGENGLKIDIHVIIPYEGLSGDQMGQIEKIFKVVYPVDDHHFKVILHYGTLVIDGVTPNMIDYFGRPYEGIAVFDGKKITVTGTLWNG
NKIIDERLINPDGSLLFRVTINGVTGWRLCERILAGSGGAETPECLVGSVPVQCLCQGLELDCDETNLRAVPSVSSNVTAMSLQWNLI
RKLPPDCFKNYHDLQKLYLQNNKITSISIYAFRGLNSLTKLYLSHNRITFLKPGVFEDLHRLEWLIIEDNHLSRISPPTFYGLNSLIL
LVLMNNVLTRLPDKPLCQHMPRLHWLDLEGNHIHNLRNLTFISCSNLTVLVMRKNKINHLNENTFAPLQKLDELDLGSNKIENLPPLI
FKDLKELSQLNLSYNPIQKIQANQFDYLVKLKSLSLEGIEISNIQQRMFRPLMNLSHIYFKKFQYCGYAPHVRSCKPNTDGISSLENL
LASIIQRVFVWVVSAVTCFGNIFVICMRPYIRSENKLYAMSIISLCCADCLMGIYLFVIGGFDLKFRGEYNKHAQLWMESTHCQLVGS
LAILSTEVSVLLLTFLTLEKYICIVYPFRCVRPGKCRTITVLILIWITGFIVAFIPLSNKEFFKNYYGTNGVCFPLHSEDTESIGAQI
YSVAIFLGINLAAFIIIVFSYGSMFYSVHQSAITATEIRNQVKKEMILAKRFFFIVFTDALCWIPIFVVKFLSLLQVEIPGTITSWVV
IFILPINSALNPILYTLTTRPFKEMIHRFWYNYRQRKSMDSKGQKTYAPSFIWVEMWPLQEMPPELMKPDLFTYPCEMSLISQSTRLN
SYSAS*

>Nanoluc-RXFP1-E277Q/D279N

MDSKGSSQKGSRLLLLLVVSNLLLCQGVVSDYKDDDDEFGSVFTLEDFVGDWRQTAGYNLDQVLEQGGVSSLFQNLGVSVTPIQRIVL
SGENGLKIDIHVIIPYEGLSGDQMGQIEKIFKVVYPVDDHHFKVILHYGTLVIDGVTPNMIDYFGRPYEGIAVFDGKKITVTGTLWNG
NKIIDERLINPDGSLLFRVTINGVTGWRLCERILAKLEFQDVKCSLGYFPCGNITKCLPQLLHCNGVDDCGNQADEDNCGDNNGWSLQ
FDKYFASYYKMTSQYPFEAETPECLVGSVPVQCLCQGLELDCDETNLRAVPSVSSNVTAMSLQWNLIRKLPPDCFKNYHDLQKLYLQN
NKITSISIYAFRGLNSLTKLYLSHNRITFLKPGVFEDLHRLEWLIIEDNHLSRISPPTFYGLNSLILLVLMNNVLTRLPDKPLCQHMP
RLHWLDLEGNHIHNLRNLTFISCSNLTVLVMRKNKINHLNENTFAPLQKLDQLNLGSNKIENLPPLIFKDLKELSQLNLSYNPIQKIQ
ANQFDYLVKLKSLSLEGIEISNIQQRMFRPLMNLSHIYFKKFQYCGYAPHVRSCKPNTDGISSLENLLASIIQRVFVWVVSAVTCFGN

IFVICMRPYIRSENKLYAMSIISLCCADCLMGIYLFVIGGFDLKFRGEYNKHAQLWMESTHCQLVGSLAILSTEVSVLLLTFLTLEKY
ICIVYPFRCVRPGKCRTITVLILIWITGFIVAFIPLSNKEFFKNYYGTNGVCFPLHSEDTESIGAQIYSVAIFLGINLAAFIIIVFSY
GSMFYSVHQSAITATEIRNQVKKEMILAKRFFFIVFTDALCWIPIFVVKFLSLLQVEIPGTITSWVVIFILPINSALNPILYTLTTRP
FKEMIHRFWYNYRQRKSMDSKGQKTYAPSFIWVEMWPLQEMPPELMKPDLFTYPCEMSLISQSTRLNSYS*

>Nanoluc-RXFP1-F54A/Y58A

MDSKGSSQKGSRLLLLLVVSNLLLCQGVVSDYKDDDDEFGSVFTLEDFVGDWRQTAGYNLDQVLEQGGVSSLFQNLGVSVTPIQRIVL
SGENGLKIDIHVIIPYEGLSGDQMGQIEKIFKVVYPVDDHHFKVILHYGTLVIDGVTPNMIDYFGRPYEGIAVFDGKKITVTGTLWNG
NKIIDERLINPDGSLLFRVTINGVTGWRLCERILAKLEFQDVKCSLGYFPCGNITKCLPQLLHCNGVDDCGNQADEDNCGDNNGWSLQ
FDKYAASYAKMTSQYPFEAETPECLVGSVPVQCLCQGLELDCDETNLRAVPSVSSNVTAMSLQWNLIRKLPPDCFKNYHDLQKLYLQN
NKITSISIYAFRGLNSLTKLYLSHNRITFLKPGVFEDLHRLEWLIIEDNHLSRISPPTFYGLNSLILLVLMNNVLTRLPDKPLCQHMP
RLHWLDLEGNHIHNLRNLTFISCSNLTVLVMRKNKINHLNENTFAPLQKLDELDLGSNKIENLPPLIFKDLKELSQLNLSYNPIQKIQ
ANQFDYLVKLKSLSLEGIEISNIQQRMFRPLMNLSHIYFKKFQYCGYAPHVRSCKPNTDGISSLE**NLLASIIQRVFVWVVSAVTCFGN**
IFVICMRPYIRSENKLYAMSIISLCCADCLMGIYLFVIGGFDLKFRGEYNKHAQLWMESTHCQLVGSLAILSTEVSVLLLTFLTLEKY
ICIVYPFRCVRPGKCRTITVLILIWITGFIVAFIPLSNKEFFKNYYGTNGVCFPLHSEDTESIGAQIYSVAIFLGINLAAFIIIVFSY
GSMFYSVHQSAITATEIRNQVKKEMILAKRFFFIVFTDALCWIPIFVVKFLSLLQVEIPGTITSWVVIFILPINSALNPILYTLTTRP
FKEMIHRFWYNYRQRKSMDSKGQKTYAPSFIWVEMWPLQEMPPELMKPDLFTYPCEMSLISQSTRLNSYS*

>Nanoluc-ECD

MDSKGSSQKGSRLLLLLVVSNLLLCQGVVSDYKDDDDEFGSVFTLEDFVGDWRQTAGYNLDQVLEQGGVSSLFQNLGVSVTPIQRIVL
SGENGLKIDIHVIIPYEGLSGDQMGQIEKIFKVVYPVDDHHFKVILHYGTLVIDGVTPNMIDYFGRPYEGIAVFDGKKITVTGTLWNG
NKIIDERLINPDGSLLFRVTINGVTGWRLCERILAKLEFQDVKCSLGYFPCGNITKCLPQLLHCNGVDDCGNQADEDNCGDNNGWSLQ
FDKYFASYYKMTSQYPFEAETPECLVGSVPVQCLCQGLELDCDETNLRAVPSVSSNVTAMSLQWNLIRKLPPDCFKNYHDLQKLYLQN
NKITSISIYAFRGLNSLTKLYLSHNRITFLKPGVFEDLHRLEWLIIEDNHLSRISPPTFYGLNSLILLVLMNNVLTRLPDKPLCQHMP
RLHWLDLEGNHIHNLRNLTFISCSNLTVLVMRKNKINHLNENTFAPLQKLDELDLGSNKIENLPPLIFKDLKELSQLNLSYNPIQKIQ
ANQFDYLVKLKSLSLEGIEISNIQQRMFRPLMNLSHIYFKKFQYCGYAPHVRSCKPNTDGISSLEDIGKPIPNPLLGLDSTHHHHHHD
ATLDPRSFLLRNPNDKYEPFWEDEEKNESGLIYIWAPLAGTCGVLLLSLVITLYCNHRNRRRVCKCPRPVVKSGDKPSLSARYV*

>Nanoluc-ECD(ΔLDLa)

MDSKGSSQKGSRLLLLLVVSNLLLCQGVVSDYKDDDDVDGSVFTLEDFVGDWRQTAGYNLDQVLEQGGVSSLFQNLGVSVTPIQRIVL
SGENGLKIDIHVIIPYEGLSGDQMGQIEKIFKVVYPVDDHHFKVILHYGTLVIDGVTPNMIDYFGRPYEGIAVFDGKKITVTGTLWNG
NKIIDERLINPDGSLLFRVTINGVTGWRLCERILAGSGDNNGWSLQFDKYFASYYKMTSQYPFEAETPECLVGSVPVQCLCQGLELDC
DETNLRAVPSVSSNVTAMSLQWNLIRKLPPDCFKNYHDLQKLYLQNNKITSISIYAFRGLNSLTKLYLSHNRITFLKPGVFEDLHRLE
WLIIEDNHLSRISPPTFYGLNSLILLVLMNNVLTRLPDKPLCQHMPRLHWLDLEGNHIHNLRNLTFISCSNLTVLVMRKNKINHLNEN
TFAPLQKLDELDLGSNKIENLPPLIFKDLKELSQLNLSYNPIQKIQANQFDYLVKLKSLSLEGIEISNIQQRMFRPLMNLSHIYFKKF
QYCGYAPHVRSCKPNTDGISSLEDIGKPIPNPLLGLDSTHHHHHHDATLDPRSFLLRNPNDKYEPFWEDEEKNESGLIYIWAPLAGTC
GVLLLSLVITLYCNHRNRRRVCKCPRPVVKSGDKPSLSARYV*

>Nanoluc-ECD(ΔLDLa/ΔLinker)

MDSKGSSQKGSRLLLLLVVSNLLLCQGVVSDYKDDDDVDGSVFTLEDFVGDWRQTAGYNLDQVLEQGGVSSLFQNLGVSVTPIQRIVL
SGENGLKIDIHVIIPYEGLSGDQMGQIEKIFKVVYPVDDHHFKVILHYGTLVIDGVTPNMIDYFGRPYEGIAVFDGKKITVTGTLWNG
NKIIDERLINPDGSLLFRVTINGVTGWRLCERILAGSGGAETPECLVGSVPVQCLCQGLELDCDETNLRAVPSVSSNVTAMSLQWNLI
RKLPPDCFKNYHDLQKLYLQNNKITSISIYAFRGLNSLTKLYLSHNRITFLKPGVFEDLHRLEWLIIEDNHLSRISPPTFYGLNSLIL
LVLMNNVLTRLPDKPLCQHMPRLHWLDLEGNHIHNLRNLTFISCSNLTVLVMRKNKINHLNENTFAPLQKLDELDLGSNKIENLPPLI
FKDLKELSQLNLSYNPIQKIQANQFDYLVKLKSLSLEGIEISNIQQRMFRPLMNLSHIYFKKFQYCGYAPHVRSCKPNTDGISSLEDI
GKPIPNPLLGLDSTHHHHHHDATLDPRSFLLRNPNDKYEPFWEDEEKNESGLIYIWAPLAGTCGVLLLSLVITLYCNHRNRRRVCKCP
RPVVKSGDKPSLSARYV*

>Nanoluc-ECD (E279Q/D279N)

MDSKGSSQKGSRLLLLLVVSNLLLCQGVVSDYKDDDDEFGSVFTLEDFVGDWRQTAGYNLDQVLEQGGVSSLFQNLGVSVTPIQRIVL
SGENGLKIDIHVIIPYEGLSGDQMGQIEKIFKVVYPVDDHHFKVILHYGTLVIDGVTPNMIDYFGRPYEGIAVFDGKKITVTGTLWNG
NKIIDERLINPDGSLLFRVTINGVTGWRLCERILAKLEFQDVKCSLGYFPCGNITKCLPQLLHCNGVDDCGNQADEDNCGDNNGWSLQ
FDKYFASYYKMTSQYPFEAETPECLVGSVPVQCLCQGLELDCDETNLRAVPSVSSNVTAMSLQWNLIRKLPPDCFKNYHDLQKLYLQN
NKITSISIYAFRGLNSLTKLYLSHNRITFLKPGVFEDLHRLEWLIIEDNHLSRISPPTFYGLNSLILLVLMNNVLTRLPDKPLCQHMP
RLHWLDLEGNHIHNLRNLTFISCSNLTVLVMRKNKINHLNENTFAPLQKLDQLNLGSNKIENLPPLIFKDLKELSQLNLSYNPIQKIQ
ANQFDYLVKLKSLSLEGIEISNIQQRMFRPLMNLSHIYFKKFQYCGYAPHVRSCKPNTDGISSLEDIGKPIPNPLLGLDSTHHHHHHD
ATLDPRSFLLRNPNDKYEPFWEDEEKNESGLIYIWAPLAGTCGVLLLSLVITLYCNHRNRRRVCKCPRPVVKSGDKPSLSARYV*

>Nanoluc-ECD

MDSKGSSQKGSRLLLLLVVSNLLLCQGVVSDYKDDDDEFGSVFTLEDFVGDWRQTAGYNLDQVLEQGGVSSLFQNLGVSVTPIQRIVL
SGENGLKIDIHVIIPYEGLSGDQMGQIEKIFKVVYPVDDHHFKVILHYGTLVIDGVTPNMIDYFGRPYEGIAVFDGKKITVTGTLWNG
NKIIDERLINPDGSLLFRVTINGVTGWRLCERILAKLEFQDVKCSLGYFPCGNITKCLPQLLHCNGVDDCGNQADEDNCGDNNGWSLQ
FDKYAASYAKMTSQYPFEAETPECLVGSVPVQCLCQGLELDCDETNLRAVPSVSSNVTAMSLQWNLIRKLPPDCFKNYHDLQKLYLQN
NKITSISIYAFRGLNSLTKLYLSHNRITFLKPGVFEDLHRLEWLIIEDNHLSRISPPTFYGLNSLILLVLMNNVLTRLPDKPLCQHMP
RLHWLDLEGNHIHNLRNLTFISCSNLTVLVMRKNKINHLNENTFAPLQKLDELDLGSNKIENLPPLIFKDLKELSQLNLSYNPIQKIQ
ANQFDYLVKLKSLSLEGIEISNIQQRMFRPLMNLSHIYFKKFQYCGYAPHVRSCKPNTDGISSLEDIGKPIPNPLLGLDSTHHHHHHD
ATLDPRSFLLRNPNDKYEPFWEDEEKNESGLIYIWAPLAGTCGVLLLSLVITLYCNHRNRRRVCKCPRPVVKSGDKPSLSARYV*

>Nanoluc-RXFP2

MDSKGSSQKGSRLLLLLVVSNLLLCQGVVSDYKDDDDVDGSVFTLEDFVGDWRQTAGYNLDQVLEQGGVSSLFQNLGVSVTPIQRIVL
SGENGLKIDIHVIIPYEGLSGDQMGQIEKIFKVVYPVDDHHFKVILHYGTLVIDGVTPNMIDYFGRPYEGIAVFDGKKITVTGTLWNG
NKIIDERLINPDGSLLFRVTINGVTGWRLCERILAGSQGSMITPSCQKGYFPCGNLTKCLPRAFHCDGKDDCGNGADEENCGDTSGWA
TIFGTVHGNANSVALTQECFLKQYPQCCDCKETELECVNGDLKSVPMISNNVTLLSLKKNKIHSLPDKVFIKYTKLKKIFLQHNCIRH
ISRKAFFGLCNLQILYLNHNCITTLRPGIFKDLHQLTWLILDDNPITRISQRLFTGLNSLFFLSMVNNYLEALPKQMCAQMPQLNWVD
LEGNRIKYLTNSTFLSCDSLTVLFLPRNQIGFVPEKTFSSLKNLGELDLSSNTITELSPHLFKDLKLLQKLNLSSNPLMYLHKNQFES

LKQLQSLDLERIEIPNINTRMFQPMKNLSHIYFKNFRYCSYAPHVRICMPLTDGISSFE**DLLANNILRIFVWVIAFITCFGNLFVIGM**
RSFIKAENTTHAMSIKILCCADCLMGVYLFFVGIFDIKYRGQYQKYALLWMESVQCRLMGFLAMLSTEVSVLLLTYLTLEKFLVIVFP
FSNIRPGKRQTSVILICIWMAGFLIAVIPFWNKDYFGNFYGKNGVCFPLYYDQTEDIGSKGYSLGIFLGVNLLAFLIIVFSYITMFCS
IQKTALQTTEVRNCFGREVAVANRFFFIVFSDAICWIPVFVVKILSLFRVEIPDTMTSWIVIFFLPVNSALNPILYTLTTNFFKDKLK
QLLHKHQRKSIFKIKKKSLSTSIVWIEDSSSLKLGVLNKITLGDSIMKPVS*

>Nanoluc-ExLink1

MDSKGSSQKGSRLLLLLVVSNLLLCQGVVSDYKDDDDVDGS**VFTLEDFVGDWRQTAGYNLDQVLEQGGVSSLFQNLGVSVTPIQRIVL**
SGENGLKIDIHVIIPYEGLSGDQMGQIEKIFKVVYPVDDHHFKVILHYGTLVIDGVTPNMIDYFGRPYEGIAVFDGKKITVTGTLWNG
NKIIDERLINPDGSLLFRVTINGVTGWRLCERILAGSQGS**MITPSCQKGYFPCGNLTKCLPRAFHCDGKDDCGNGADEENC**GDTSGWA
TIFGKYFATVHGNANSVALTQECFLKQYPQCCDCKETELECVNGDLKSVPMISNNVTLLSLKKNKIHSLPDKVFIKYTKLKKIFLQHN
CIRHISRKAFFGLCNLQILYLNHNCITTLRPGIFKDLHQLTWLILDDNPITRISQRLFTGLNSLFFLSMVNNYLEALPKQMCAQMPQL
NWVDLEGNRIKYLTNSTFLSCDSLTVLFLPRNQIGFVPEKTFSSLKNLGELDLSSNTITELSPHLFKDLKLLQKLNLSSNPLMYLHKN
QFESLKQLQSLDLERIEIPNINTRMFQPMKNLSHIYFKNFRYCSYAPHVRICMPLTDGISSFE**DLLANNILRIFVWVIAFITCFGNLF**
VIGMRSFIKAENTTHAMSIKILCCADCLMGVYLFFVGIFDIKYRGQYQKYALLWMESVQCRLMGFLAMLSTEVSVLLLTYLTLEKFLV
IVFPFSNIRPGKRQTSVILICIWMAGFLIAVIPFWNKDYFGNFYGKNGVCFPLYYDQTEDIGSKGYSLGIFLGVNLLAFLIIVFSYIT
MFCSIQKTALQTTEVRNCFGREVAVANRFFFIVFSDAICWIPVFVVKILSLFRVEIPDTMTSWIVIFFLPVNSALNPILYTLTTNFFK
DKLKQLLHKHQRKSIFKIKKKSLSTSIVWIEDSSSLKLGVLNKITLGDSIMKPVS*

>Nanoluc-ExLink2

MDSKGSSQKGSRLLLLLVVSNLLLCQGVVSDYKDDDDVDGS**VFTLEDFVGDWRQTAGYNLDQVLEQGGVSSLFQNLGVSVTPIQRIVL**
SGENGLKIDIHVIIPYEGLSGDQMGQIEKIFKVVYPVDDHHFKVILHYGTLVIDGVTPNMIDYFGRPYEGIAVFDGKKITVTGTLWNG
NKIIDERLINPDGSLLFRVTINGVTGWRLCERILAGSQGS**MITPSCQKGYFPCGNLTKCLPRAFHCDGKDDCGNGADEENC**GDTSGWA
TIFGKYFASYYTVHGNANSVALTQECFLKQYPQCCDCKETELECVNGDLKSVPMISNNVTLLSLKKNKIHSLPDKVFIKYTKLKKIFL
QHNCIRHISRKAFFGLCNLQILYLNHNCITTLRPGIFKDLHQLTWLILDDNPITRISQRLFTGLNSLFFLSMVNNYLEALPKQMCAQM
PQLNWVDLEGNRIKYLTNSTFLSCDSLTVLFLPRNQIGFVPEKTFSSLKNLGELDLSSNTITELSPHLFKDLKLLQKLNLSSNPLMYL
HKNQFESLKQLQSLDLERIEIPNINTRMFQPMKNLSHIYFKNFRYCSYAPHVRICMPLTDGISSFE**DLLANNILRIFVWVIAFITCFG**
NLFVIGMRSFIKAENTTHAMSIKILCCADCLMGVYLFFVGIFDIKYRGQYQKYALLWMESVQCRLMGFLAMLSTEVSVLLLTYLTLEK
FLVIVFPFSNIRPGKRQTSVILICIWMAGFLIAVIPFWNKDYFGNFYGKNGVCFPLYYDQTEDIGSKGYSLGIFLGVNLLAFLIIVFS
YITMFCSIQKTALQTTEVRNCFGREVAVANRFFFIVFSDAICWIPVFVVKILSLFRVEIPDTMTSWIVIFFLPVNSALNPILYTLTTN
FFKDKLKQLLHKHQRKSIFKIKKKSLSTSIVWIEDSSSLKLGVLNKITLGDSIMKPVS*

>RXFP2$_{(1\text{-}65)}$-ExLink

MHHHHHHHHSSGQYKLALNGKTLKGETTTEAVDAATAEKVFKQYANDNGVDGEWTYDDATKTFTVTELVPRGS**MITFSCQ**
KGYFPCGNLTKCLPRAFHCDGKDDCGNGADEENCGDTSGWATIFGKYFASYYTVHGNANSVALTQEQYKLALNGKTLKGE
TTTEAVDAATAEKVFKQYANDNGVDGEWTYDDATKTFTVTE*

Transparent Methods

Cell culture and transfection

HEK293T cells (ATCC #CRL-1573; American Type Tissue Culture Collection) and a HEK293A cell line with CRISPR deletion of GNAS (HEK293A $\Delta G_{\alpha s}$; (Stallaert et al., 2017)) were grown in complete medium (Dulbecco's Modified Eagle Medium (DMEM; Sigma-Aldrich) supplemented with 10% FBS, 1% L-glutamine, and 1% penicillin/streptomycin) and maintained 37 °C incubators with 5% CO_2. For receptor expression, cells were first seeded into 6-well plates at a density of 6 X 10^5 cells/well. The following day, cells were transfected with receptor DNA using LipofectAMINE 2000 (Invitrogen, Carlsbad, CA), usually with 10-30 ng DNA per well unless otherwise stated. Nanoluc RXFP2 and variants were transfected using polyethylenimine (PEI; Sigma-Aldrich) with 500 ng DNA per well and a ratio of 4.5 µl PEI per µg of DNA. 24-hours post-transfection, cells were resuspended and seeded into 96-well optiplates for assay the following day.

TamRLX synthesis

Individual A- and B-chains of H2 relaxin with appropriate regioselective S-protection were synthesized using a CEM Liberty peptide synthesizer (Akhter Hossain et al., 2008). Upon complete coupling and Fmoc deprotection of the final amino acid, glutamine (Q), at the N-terminus of the A-chain sequence, the amine-reactive fluorophore 5(6)-TAMRA succinimidyl ester (Anaspec) was attached using manual coupling procedure. Following final TFA cleavage and purification of the crude peptides (TAMRA A-chain and B-chain), stepwise formation of the three disulfide bonds was conducted via oxidation, thiolysis and iodolysis consecutively (Akhter Hossain et al., 2008). The final TAMRA-labelled relaxin, TamRLX, was subjected to comprehensive characterization by RP-HPLC and MALDI-TOF mass spectrometry to confirm its high purity and correct molecular mass (m/z calculated for TamRLX $[M+Na]^+$, 6415.456, found 6419.70).

Receptor construct cloning

All receptor constructs were cloned in pcDNA3.1/Zeo (Invitrogen) plasmids and contained an N-terminal FLAG tag as well as the non-native bovine prolactin signal peptide to aid receptor expression as previously described for both RXFP1 and ECD-only (previously termed 7BP) (Hsu et al., 2002). The gene for Nanoluc was synthesised (GenScript Corp., Nanjing, China) and inserted between the FLAG tag and LDLa module via the insertion of an EcoRI restriction site using standard restriction enzyme based cloning methods. For RXFP2 and constructs in which the LDLa and/or the linker domain had been removed, PCR products encoding the relevant receptor and stop codon were inserted C-terminally to the Nanoluc in a pcDNA3.1/Zeo vector containing signal peptide, FLAG tag and Nanoluc. Receptor mutations (F54A/58A and E277Q/D279N) were achieved by QuikChange mutagenesis with PrimeStar polymerase (Takara Clontech, Mountain View, CA) according to manufacturer's instructions and similarly to previously described (Sethi et al., 2016). RXFP2 extended linker (ExLink) chimeras were made according to the method described in (Liu and Naismith, 2008) whereby primers were designed with short overlapping sections with T_m 5-10 ° C lower than that of non-overlapping sections in either direction. PCR reaction mixes of 50 µl were subjected to the following protocol: 5 min at 95 °C; 12 cycles of 95 °C (1 min), 53 °C (1 min), 68 °C (12 min); 1 min at 43 °C followed by a further extension step at 68 °C for 30 min, and 4 °C hold. All receptor constructs were verified by sequencing across the entirety of the ORF, and full amino acid sequences of receptor constructs are provided in supplemental information.

cAMP reporter gene assay

cAMP activity in HEK293T cells expressing receptors in response to ligand stimulation was measured using a pCRE β-gal reporter gene assay (Chen et al., 1995). For RXFP1 and mutants HEK293T cells were prepared for assay according to transfection methods described above, but were transfected with 50 ng / well of receptor DNA and 2 μg/well of pCRE β-gal DNA. RXFP2 and ExLink chimeras were tested using conditions described in (Bruell et al., 2017). Briefly, cells were seeded at 25,000 cells per well in 96-well Cellbind plates (Corning) and the following day transfected with LipofectAMINE 2000 at 0.5 μl per well and 0.25 μg DNA per well, divided in proportions of 1:2:5 of receptor, β-gal and pcDNA3.1 (empty) vector. For experiments in which relaxin was compared to TamRLX, a HEK293T cell line stably expressing RXFP1 and pCRE β-gal was instead used. On the day following seeding into 96-well plates, cells were treated with 5 μM forskolin (as a receptor independent control for response normalisation) or increasing concentrations of relaxin in complete medium. For assays of ML290-induced cAMP activity, dilutions were prepared in dimethyl sulphoxide (DMSO) and added to minimal media (DMEM containing 0.5% foetal bovine serum, 1% L-glutamine, 1% penicillin/streptomycin) such that wells contained 1% final DMSO concentration. Cells were incubated with ligands at 37 °C for 6 h, after which media was aspirated and the cells frozen at -80 °C overnight. The amount of cAMP-driven β-gal expression was determined by lysing cells in 25 μL/well of assay buffer 1 (10 mM Na_2PO_4, pH 8.0, 0.2 mM $MgSO_4$, 0.01 mM $MnCl_2$) for 10 min, followed by 100 μL/well of assay buffer 2 (100 mM Na_2PO_4, pH 8.0, 2 mM $MgSO_4$, 0.1 mM $MnCl_2$, 0.5 % Triton X-100, 40 mM β-mercaptoethanol) for a further 10 min before the addition of 25 μL/well of enzyme substrate solution (1 mg / ml chlorophenol red β-D-galactopyranoside in assay buffer 2). The absorbance of each well was monitored using a Benchmark Plus Microplate Reader (Bio-Rad, Hercules, CA) at 570 nm. Experiments were performed in triplicate at least 3 times, and data were pooled and presented as percentages of the response induced by 5 μM forskolin. Data was fit to a three-parameter sigmoidal dose-response curve using GraphPad Prism to yield pEC_{50} and E_{max} values. Statistical significance was assessed by ordinary one-way analysis of variance (ANOVA) and uncorrected Fisher's least squares difference (LSD) multiple comparison test.

BRET measurements

All BRET measurements were performed in POLARstar Omega plate reader (BMG Labtech) equipped with emission filters for the 'donor' (410-490 nm) and 'acceptor' (>610 nm long-pass) luminescence emission. BRET ratio was defined as the ratio of the acceptor emission over the donor emission.

NanoBRET saturation binding assays

Transfected cells in 96-well plates (prepared according to transfection methods described above) were first washed with 100 μL/well of PBS (pH 7.4) and incubated with 90 μL /well of assay buffer (Phenol-red free DMEM containing 10% FBS, 1% L-glutamine, 1% penicillin/streptomycin, 25 mM HEPES, pH 7.4 for RXFP1 and variants; or 20mM HEPES, pH 7.5, 1.5 mM $CaCl_2$, 50 mM NaCl containing 1% BSA for RXFP2 and variants) containing varying concentrations of TamRLX (with or without an excess of unlabelled relaxin to determine non-specific binding signal) for 90 minutes, either at room temperature or 37 °C. Following incubation, 10 μL/well of assay buffer containing a 1:50 dilution Nano-Glo luciferase substrate (Promega Corporation, Fitchburg, WI) was added, followed by BRET measurement. BRET ratios were fit using a "One-site – Total and nonspecific binding" saturation binding equation in GraphPad Prism (La Jolla, CA) to yield dissociation constants (K_d). Statistical significance was assessed by ordinary one-way ANOVA and uncorrected Fisher's LSD multiple comparison test of pooled pKd values.

NanoBRET association assays

Transfected cells in 96-well plates (prepared according to transfection methods described above) were first washed with 100 µL/well of PBS (pH 7.4) and then 100 µL/well of assay buffer containing a 1:500 dilution of Nano-Glo luciferase substrate was added. BRET measurements were performed in a POLARStar Omega plate reader every minute for 15 minutes, before manual addition of 50 µL of assay buffer containing varying concentrations of TamRLX (or vehicle only) and a 1:500 dilution of Nano-Glo luciferase substrate, with further BRET measurements every minute for 60 more minutes.

NanoBRET dissociation assays

Transfected cells in 96-well plates (prepared according to transfection methods described above) were first washed with 100 µL / well of PBS (pH 7.4), then 100 µL of assay buffer containing a 1:500 dilution of Nano-Glo luciferase substrate (plus or minus TamRLX) was added, with BRET measurement every minute. For RXFP1 experiments at room temperature, 1 nM TamRLX was used and dissociation was initiated after 60 minutes of incubation with BRET measurements by removal of buffer in all wells and replacement with assay buffer containing a 1:500 dilution of Nano-Glo luciferase substrate and 10 µM unlabelled relaxin (to normalise data, "non-dissociation" wells were included in which the same concentration of TamRLX was added back, without the unlabelled relaxin). For RXFP2 experiments 13 nM TamRLX was used and due to the faster speed of dissociation, 2 µM unlabelled INSL3 was added directly into wells after 15 minutes of incubation with BRET measurements. For experiments at 37 °C, 5 nM of TamRLX was used and dissociation was instead initiated by automated injection of 3 µL/well of 1 mg/mL unlabelled relaxin (to a final concentration of roughly 5 µM) after 30 minutes of BRET measurements. Data was pooled and presented as mean ± SEM of at least three independent experiments each performed in triplicate. Dissociation was normalized to wells containing TamRLX with no dissociation (100%) and buffer containing vehicle only (0%), all in the presence of substrate. Curves were fit using GraphPad Prism with a one-site and then a two-site exponential decay function, with goodness of fit being assessed by observation of associated mean residual plots. Off-rates were extracted as k_{off} for one-site curves, and $k_{off\ FAST}$, and $k_{off\ SLOW}$ along with % Fast for two-site curves. Where applicable, statistical significance was calculated using ordinary one-way ANOVA and uncorrected Fisher's LSD multiple comparison test.

Protein expression and purification

Our NMR analysis made use of the same construct described and characterized by us in (Bruell et al., 2017), which consists of the first 65 residues of human RXFP2, constituting the LDLa module and linker, with residue Pro4 mutated to Phe to give a homogeneous spectrum without interfering with activity, and a C-terminal GB1 solubility and stabilization tag. We refer to this construct as $RXFP2_{(1-65)}$ and append the name ExLink to denote the insertion of seven RXFP1 linker residues (see supporting information). We inserted linker residues into $RXFP2_{(1-65)}$-ExLink in two rounds of site-directed mutagenesis, as described above for the whole receptor. Once the sequence had been confirmed the construct was expressed in BL21(DE3)-*trxB* cells as described in (Bruell et al., 2017). Protein purification proceeded as previously described, making use of the N-terminal HIS tag which was bound to Talon Superflow resin (Takara Clontech), then washed and eluted in 400 mM imidazole in 20 mM Tris-HCl (pH7.4), 150 mM NaCl. The eluted protein was then re-folded overnight in a mixed redox reaction, and the following night the HIS tag and N-terminal GB1 tag were removed with 5 units of thrombin per mg of protein. A run through an Agilent Zorbax 300SB-C18 column on reverse phase high performance liquid chromatography (RP-HPLC) further purified

the final product which was verified by mass spectrometry for correct molecular weight and purity before being lyophilized and stored at -20 °C.

NMR Spectroscopy

NMR experiments were all performed at 25 °C on a 700 MHz Bruker Avance HDIII or Bruker Avance II HD 800 MHz spectrometer each equipped with a triple resonance cryoprobe. Proteins were dissolved in 50 mM imidazole, 10 mM $CaCl_2$ at pH 6.8. Backbone resonances ($^{13}C\alpha$, $^{13}C\beta$, $^{13}C'$, ^{15}N and NH) of the residues of $RXFP2_{(1-65)}$-ExLink were assigned from 3D HNCACB, HN(CO)CACB, HNCO and HN(CA)CO experiments using non-uniform sampling (NUS) at 800 MHz. For NUS, sampling schedules were generated using poisson gap sampler with 10% of the total number of points collected for all the 3D NMR experiments (Hyberts et al., 2010). Spectra were reconstructed with compressed sensing algorithm using qMDD (Kazimierczuk and Orekhov, 2011) and processed using NMRPipe (Delaglio et al., 1995) as described in (Sethi et al., 2016) and data analyzed in SPARKY (Lee et al., 2015). The chemical shift assignments for $RXFP2_{(1-65)}$-ExLink have been deposited in the BioMagResBank (http://www.bmrb.wisc.edu) under the accession number 27601. Samples for titrations were dialyzed in the same buffer. Chemical shift and intensity changes were monitored via the acquisition of 2D ^{1}H-^{15}N Heteronuclear Single Quantum Coherence (HSQC) as described for $RXFP1_{(1–72)}$ in (Kay et al., 1989), using increasing concentrations of each titrant against 50 μM $RXFP2_{(1-65)}$-ExLink.

Supplemental References

AKHTER HOSSAIN, M., BATHGATE, R. A., KONG, C. K., SHABANPOOR, F., ZHANG, S., HAUGAARD-JÖNSSON, L. M., ROSENGREN, K. J., TREGEAR, G. W. & WADE, J. D. 2008. Synthesis, Conformation, and Activity of Human Insulin-Like Peptide 5 (INSL5). *ChemBioChem,* 9**,** 1816-1822.

CHEN, W., SHIELDS, T. S., STORK, P. J. & CONE, R. D. 1995. A colorimetric assay for measuring activation of Gs- and Gq-coupled signaling pathways. *Anal. Biochem.,* 226**,** 349.

DELAGLIO, F., GRZESIEK, S., VUISTER, G. W., ZHU, G., PFEIFER, J. & BAX, A. 1995. NMRPipe: a multidimensional spectral processing system based on UNIX pipes. *J Biomol NMR,* 6**,** 277-93.

HYBERTS, S. G., TAKEUCHI, K. & WAGNER, G. 2010. Poisson-gap sampling and forward maximum entropy reconstruction for enhancing the resolution and sensitivity of protein NMR data. *J Am Chem Soc,* 132**,** 2145-7.

KAY, L. E., TORCHIA, D. A. & BAX, A. 1989. Backbone dynamics of proteins as studied by nitrogen-15 inverse detected heteronuclear NMR spectroscopy: application to staphylococcal nuclease. *Biochemistry,* 28**,** 8972-8979.

KAZIMIERCZUK, K. & OREKHOV, V. Y. 2011. Accelerated NMR spectroscopy by using compressed sensing. *Angewandte Chemie International Edition,* 50**,** 5556-5559.

LEE, W., TONELLI, M. & MARKLEY, J. L. 2015. NMRFAM-SPARKY: enhanced software for biomolecular NMR spectroscopy. *Bioinformatics,* 31**,** 1325-7.

LIU, H. & NAISMITH, J. H. 2008. An efficient one-step site-directed deletion, insertion, single and multiple-site plasmid mutagenesis protocol. *BMC Biotechnol,* 8**,** 91.